3-D GEOMETRICAL RECONSTRUCTION AND FLEXURAL MODELING OF COLVILLE FORELAND BASIN, NORTHERN ALASKA

by

Muhammad Hassan Quddusi

APPROVED BY SUPERVISORY COMMITTEE:

_____

Mortaza Pirouz, Chair

_____

Robert J. Stern

_____

Hejun Zhu

To my beloved wife and son:

Arooba Hassan, Musa Hassan Quddusi

3-D GEOMETRICAL RECONSTRUCTION AND FLEXURAL MODELING OF COLVILLE FORELAND BASIN, NORTHERN ALASKA

by

MUHAMMAD HASSAN QUDDUSI, BS,MS

THESIS

Presented to the Faculty of

The University of Texas at Dallas

in Partial Fulfillment

of the Requirements

for the Degree of

MASTER OF SCIENCE IN

GEOSCIENCES

THE UNIVERSITY OF TEXAS AT DALLAS

May 2020

ACKNOWLEDGMENTS

I would like to thank my committee, Drs. Mortaza Pirouz, Robert Stern and Hejun Zhu, for their continued support and guidance in my continuing education. Mortaza always challenged me and fundamentally changed the way that I think. Robert Stern offered me encouragement as well as support and never stopped believing in me. Hejun provided me many opportunities to learn about geophysics.

I would like to thank Mortaza Pirouz for his assistance in running models and for his continued collaboration on this project. Thank you to the UTD Department of Geosciences for their support; they truly have become a part of my extended family. Finally, thank you to my wife, Arooba Hassan, for supporting me during the graduate studies.

April 2020

3-D GEOMETRICAL RECONSTRUCTION AND FLEXURAL MODELING OF COLVILLE FORELAND BASIN, NORTHERN ALASKA

Muhammad Hassan Quddusi, MS
The University of Texas at Dallas, 2020

Supervising Professor: Mortaza Pirouz

Brooks Range orogeny initiated in response to the collision of Arctic Alaska with an oceanic arc in Jurassic to early Cretaceous, and the Colville basin formed as a result of loading from the range topography. In this study Colville basin geometry is constrained and spatiotemporal variations of deflection is modeled in northern Alaska in order to estimate the elastic thickness (Te) of the lithosphere beneath the Colville foreland basin. Previous studies show that the effective elastic thickness of the Colville Basin in the northern Alaska region is 65 km which seems overestimated. That is because, the depth of frequent earthquakes dramatically reduces at 25 km under the Brooks Range and Colville foreland and wavelength of the Colville foreland is shorter than what one can expect for a plate with 65 km elastic thickness. To address these contrasting observations, a 3D flexural model technique is used to provide an accurate elastic thickness of northern Alaska lithosphere. The geometry of the Colville basin is characterized by using subsurface data and available structure maps, where the maximum depth reaches to 8 km towards the southwest of the basin. Flexural deflection of the northern Alaskan plate is modeled by various parameters (e.g., density, subsurface load), and results are compared to the observed data to optimize modeling

results. The applied loads include basin and topographic loads along with crustal root loads with a ratio of 4.5 times to modern topography. Calculated elastic thickness is about 16 km and an average misfit between the model and observation is less than 3% and spans 83000 km^2 of the basin. The results of this study indicate that the Colville basin geometry is mainly controlled by the loads of the Brooks Range and basin deposits and any other additional loads or density anomalies in the crust are not required for deflection of the Colville foreland basin.

TABLE OF CONTENTS

ACKNOWLEDGEMENTS.....v

ABSTRACT vi

LIST OF FIGURES.....x

LIST OF TABLES.....xii

CHAPTER 1 INTRODUCTION 1

CHAPTER 2 GEOLOGIC HISTORY OF NORTHERN ALASKA 6

2.1 Tectonic Evolution..... 6

2.2 Tectono-stratigraphic Sequences 8

2.3 Geometry of Colville Foreland Basin 10

2.4 Crustal Structure of Northern Alaska 13

CHAPTER 3 FLEXURE MODELING OF NORTHERN ALASKA..... 15

3.1 Definition of Foreland Basin 15

3.2 Strength of Lithospheric Plate 15

3.3 Flexure Model Description 17

3.4 Available Data 20

3.5 Modeling Workflow..... 23

CHAPTER 4 GEOPHYSICAL MODELING OF NORTHERN ALASKA 27

4.1 Concept of Gravity Anomalies 27

4.2 Concept of Isostacy 30

4.3 Elastic Thickness from Gravity Data 31

4.4 Available Data 31

4.5 Modeling Workflow 32

CHAPTER 5 RESULTS AND DISCUSSION 36

5.1 Flexure of Colville Basin 36

5.2 Elastic Thickness (Te) 39

5.3 Implication for Subsurface Loads 41

5.4 Gravity and Flexural Support 42

5.5 Earthquake Observation 51

CHAPTER 6 CONCLUSION 54

REFERENCES 57

BIOGRAPHICAL SKETCH 60

CURRICULUM VITAE

LIST OF FIGURES

Figure 1. Modern plate setting of northern Alaska. 2

Figure 2. (a) Map of the seismic derived crust-mantle boundary. 3

Figure 3. Late-Jurassic to Early-Cretaceous tectonic setting of northern Alaska. 7

Figure 4. Mid-Jurassic to Late-Cretaceous tectonic setting of northern Alaska. 7

Figure 5. Stratigraphic column of Colville basin.. 11

Figure 6. LCU Correlation. 12

Figure 7. Bouguer anomaly map 14

Figure 8. Schematic Flexural model. 18

Figure 9. Display of 2D seismic lines. 21

Figure 10. Cross-section of LCU correlation. 22

Figure 11. Pratt and Airy isostatic compensation schematic model. 30

Figure 12. Vertical density variations 34

Figure 13. Predicted and observed foreland depths. 37

Figure 14. Cross-sections showing observed and predicted flexure 38

Figure 15. Root Mean Square Error (RMSE) 40

Figure 16. Free-air anomaly map 43

Figure 17. Observed and predicted free-air anomaly 45

Figure 18. Free-air anomaly from Moho boundary. 46

Figure 19. A comparison of Moho derived free-air anomalies 47

Figure 20. Free-air anomaly cross-sections. 48

Figure 21. Comparison between observed and predicted Moho 50

Figure 22. Earthquake frequency distribution histogram. 52

Figure 23. Location of earthquake depth and magnitude. 53

LIST OF TABLES

Table 1. Elastic parameters used in flexural modeling…….....…….....36

Table 2. Summary of flexure modeling ……...……...…….....49

CHAPTER 1

INTRODUCTION

The North Slope of Alaska is underlain by an east-west trending Colville foreland basin (Figure 1). The basin formed in response to Brooks Range orogeny that initiated due to south-directed (present coordinates) collision of Arctic Alaska continental terrane with an oceanic island arc in Jurassic to Early Cretaceous (Box, 1985; Bird and Molenaar, 1992; Moore et al., 1994; Houseknecht, 2019). The Brooks Range separates southward flanking Yukon-Koyukuk basin that extends into western Alaska (Patton and Box, 1989). Previous studies on the Colville basin show that sediment infill mainly occurred in the Cretaceous to the Tertiary as sediments derived from the adjacent Brooks Range. Foreland basins in collisional zones are associated with down warping flexure of the lithosphere as a result of thrust sheets and accumulating sediment loads (e.g. Beaumont, 1981; Karner and Watts, 1983; DeCelles, 2012). The subsurface load may also contribute either by static or dynamic forces. The static force is mainly accommodated by density variations of the subducting slab and the associated lithospheric root underneath the orogen. The dynamic forces are mostly supported by mantle flow (Royden, 1988; Garcia-Castellanos, 2002; Pirouz et al., 2017). Both surface and buried loads are associated with the mechanical behavior of the lithosphere underlying the foreland basin. Therefore, foreland basin architecture offers essential insights into the geodynamics of the lithosphere.

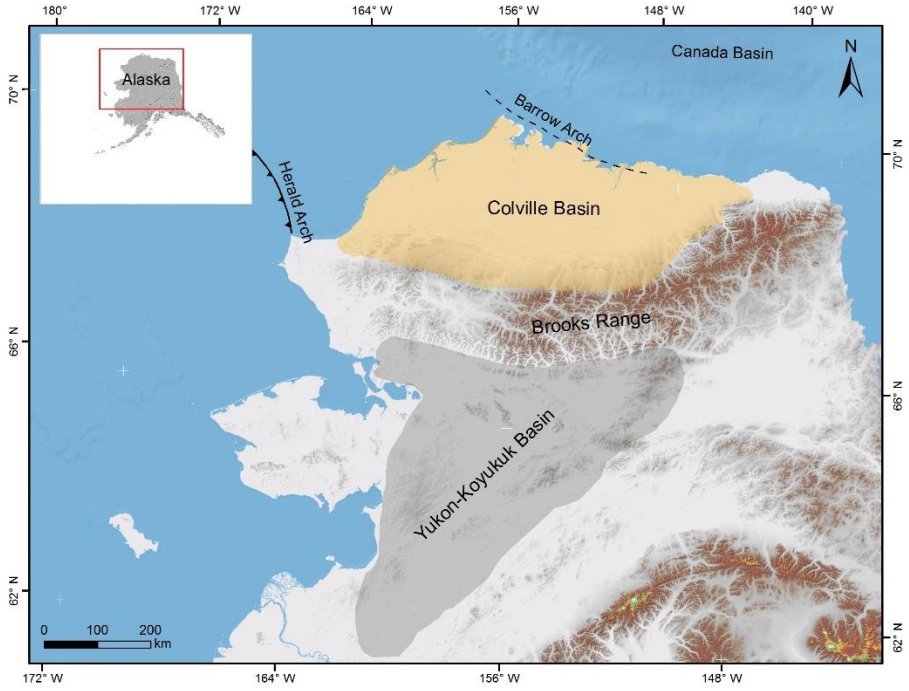

Figure 1. Modern plate setting of northern Alaska. Brooks Range fold and thrust belt are flanked on the north and south by Colville and Yukon-Koyukuk foreland basins. The depth and flexure of the Colville foreland basin are modeled in this study.

For further investigation of the foreland basin architecture, gravity data of the basin has been investigated. Buried loads associated with flexure of lithosphere can be described by Bouguer gravity anomalies that hold valuable insights into the mass excess or deficit under the mountain or foreland basin (Karner and Watts, 1983; Molnar and Lyon-Caen, 1988; Royden, 1988). Compared to the gravity measurements that would be expected in isostatic equilibrium, the Brooks Range and Colville foreland basin shows low gravity values indicating mass deficit beneath the belt and basin (Nunn et al., 1987). More recent 3D forward modeling of crustal density variations and Bouguer anomalies of Alaska is carried out by Torne et al. (2020) and their results highlight thick crust about 45 km beneath the Brooks Range and beneath the Colville basin it gradually decreases

by a few kilometers (Figure 2). Using gravity and topographic data Nunn et al. (1987) modeled a simple 2-D flexure of Colville foreland basin in northern Alaska. Their results suggested that the topographic and basin loads are not enough to produce observed deflection in the basin. They inferred that an additional subsurface load is required to produce present day basin geometry.

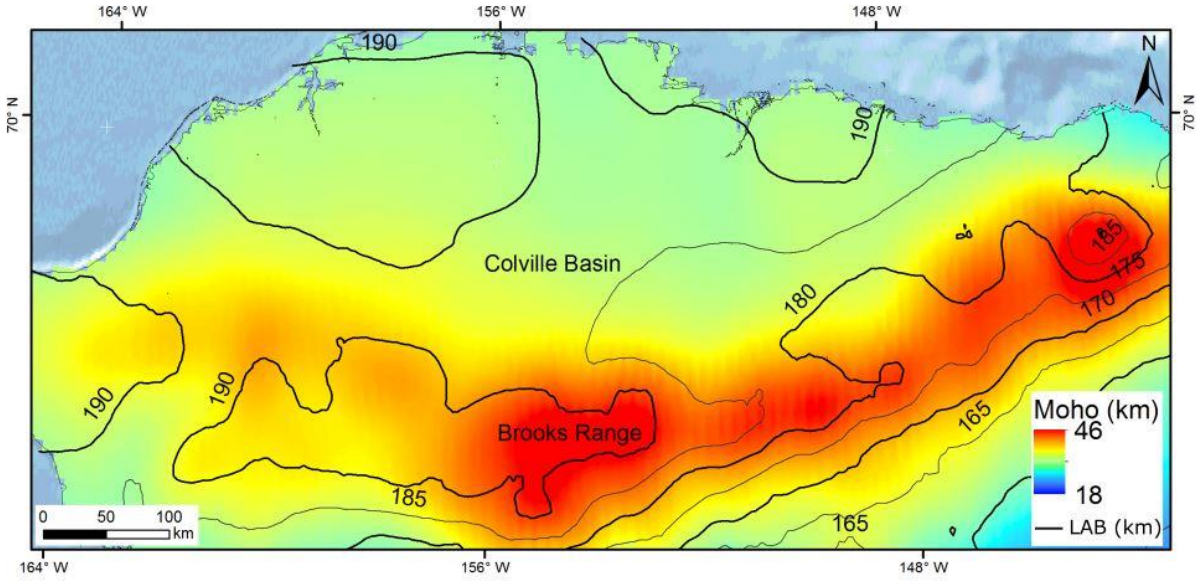

Figure 2. (a) Map of the seismic derived crust-mantle boundary (color shading) with contours indicating lithosphere-asthenosphere boundary (LAB) derived from (Torne et al., 2020).

Geometry and sedimentary record of the Colville basin play a significant role to explore dynamics of the northern Alaska and geomechanics of the lithosphere. Isostatic balance of lithosphere is more realistically described by flexural compensation between topographic load and subsidence in the foredeep (DeCelles and Giles, 1996; Turcotte and Schubert, 2002; Kearey et al., 2009). As the sediments shed from the range, they accumulate in the adjacent depressions created by the topographic load and orogenic root. Lithospheric deflection and geometry of the foreland basins

are mainly controlled by the size and width of the orogen, and elastic thickness (Te) of the plate where the basin is developed on.

Recent studies show that 3D flexural solutions constrain better results for basin geometry, spatial/temporal variations in crustal parameters, and elastic thickness compared with 2D models by applying a more realistic load of topography and basin deposits (Pirouz et al., 2017; Curry et al., 2019). A recent reconstruction of the Arabian plate deflection using a 3D approach shows that the topographic and basin loads along with the weight of crustal root models accurate foreland basin geometry (Pirouz et al., 2017). In addition, they show that using geological observations in flexural forward modeling reconstructs better estimates for lithospheric elastic thickness to compare with gravity data. In contrast, observed gravity offers better insights for calculating the amount of load posed by the crustal root.

Comparison between Colville basin's wavelength with modern systems like Zagros and Taiwan enables us to have the first order of lithospheric elastic thickness estimation. The Zagros foreland basin width is approximately 450 km and elastic thickness about 50 km. In the Taiwan foreland basin, basin width is 110 km and elastic thickness is 13 km (Lin and Watts, 2002, Pirouz et al., 2017). The elastic thickness for the Colville basin with 200 km width is identified 65 km (Nunn et al., 1987), however by comparison with other foreland basins; it seems reported elastic thickness for this basin is probably overestimated with respect to the basin wavelength. Furthermore, seismic events mostly take place in the brittle zone of the crust; therefore, seismicity of terranes can also be used to estimate the elastic thickness of the lithosphere. In the North Slope region of Alaska,

the frequency of earthquakes drops dramatically at a depth of 25 km, which is in contrast with the proposed 65 km of elastic thickness by Nunn et al., (1987).

The purpose of this study is to address how geometry of the Colville foreland basin relates to orogenic loads posed by the Brooks Range fold and thrust belt. To obtain 3D geometry of the Colville foreland basin, subsurface data (seismic and well data provided by USGS) and published structural maps of the base of foreland (Bird and Houseknecht, 2011) characterized by a regional unconformity separating foreland deposits from passive shelf margin has been used. Using the flexural modeling results the elastic thickness (Te) of the lithosphere underlying North Slope of Alaska is estimated and the possibility of additional subsurface load and influence of the southern Alaska subduction zone in the architecture of the Colville basin geometry is investigated. Geophysical investigation in this study includes calculation of the surface free-air anomaly (FAA) using published Moho depth (Torne et al., 2020), and the flexural modeling result and correlation of calculated versus observed gravity anomalies (Bonvalot et al., 2012). The flexural model of the lithosphere underneath the North Slope of Alaska describes a thickened crust and sediment load, which fits best to the observed geometry of the foreland as well as the gravity data. A simple 3D elastic plate flexural bending model has been used which accurately describes the continental lithosphere.

CHAPTER 2

GEOLOGIC HISTORY OF NORTHERN ALASKA

2.1 Tectonic Evolution

Alaska is a landmass formed by an amalgamation of several litho-tectonic terranes of varying origins that were thoroughly assembled by Late Cretaceous (Plafker and Berg, 1994a; Fuis et al., 2008; Moore and Box, 2016). During the Jurassic and Early-Cretaceous, two major tectonic events dominated in this region. In the Early-Cretaceous the Arctic Alaska terrane collided with an oceanic arc-continent complex (Figure 3) and bent downward in response to the collision. At the same time on the opposite side of the Alaska terrane, onset of rifting occurred that would eventually lead to the opening of present-day Canada basin (Mayfield et al., 1983; Sweeney, 1985). The outline in the background (Figure 3) is the present-day geographical boundary that shows the relative position of the Arctic Alaska and the oceanic arc terranes as they began to collide. By the Mid-Cretaceous, the collision resulted in the formation of the Brooks Range fold and thrust mountain belt and the associated foredeeps on its both sides (Figure 4). As the orogen evolved it also rotated counterclockwise subsequently with the opening of the Canada basin. Although the counterclockwise rotation of the Arctic Alaska terrane and similarly other terranes in this region have been a topic of debate, but nonetheless it is the most widely accepted and plausible explanation of present-day tectonic setting. Using geological and geophysical data (Embry, 1990) also supported the hypothesis of counterclockwise rotation of northern Alaska terranes away from the Canada basin. An extensive discussion of all the terrane nomenclature of Alaska is beyond the scope of this study; the reference is made to (Moore et al., 1994; Plafker and Berg, 1994b; Fuis et

al., 1997; Moore and Box, 2016) where a compilation of most of the existing literature on the subject can be found.

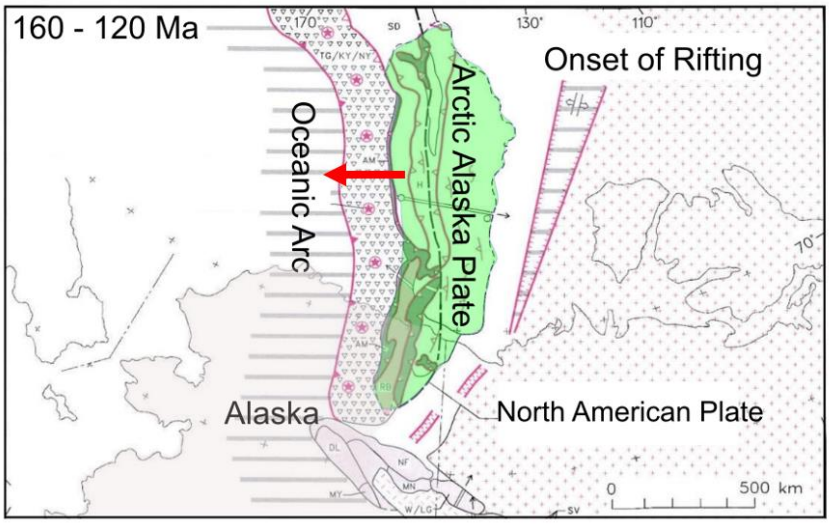

Figure 3. Late-Jurassic to Early-Cretaceous tectonic setting of northern Alaska. Red arrow indicates the direction of movement of Arctic Alaska terrane towards oceanic arc complex. The present-day geographical boundaries are outlined in the background.

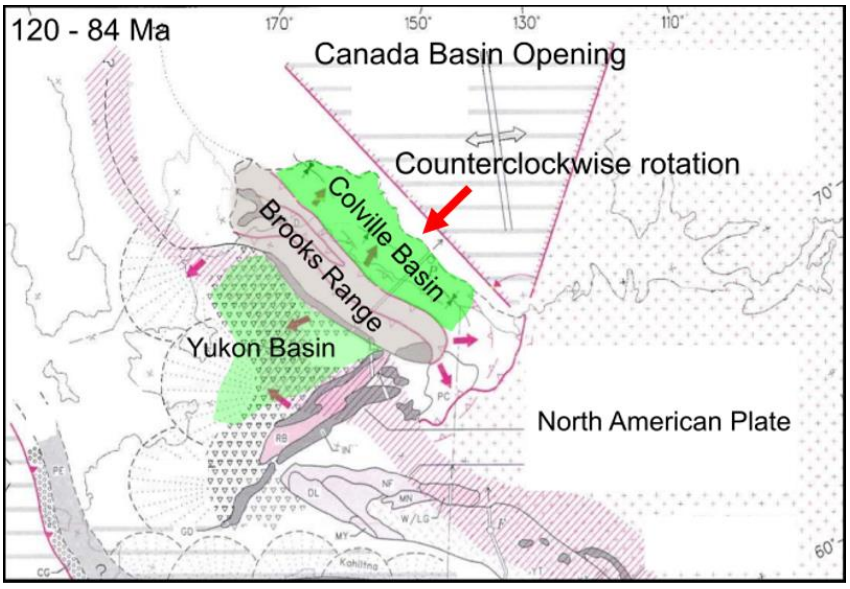

Figure 4. Mid-Jurassic to Late-Cretaceous tectonic setting of northern Alaska. Red arrow indicates the direction of movement of Arctic Alaska terrane towards oceanic arc complex due to counterclockwise rotation as a result of opening of Canada basin.

Present-day North Slope of Alaska (Figure 1) consists of the Arctic Alaska terrane that constitutes the Brooks Range fold and thrust belt and the Colville foreland basin north of the Brooks Range (Miller, 1994; Moore et al., 1994; Plafker and Berg, 1994; Bird, 2001). Towards the south of the Brooks Range, lies a Cretaceous age foreland basin called Yukon-Koyukuk basin that extends into the western Alaska region (Patton and Box, 1989). The Brooks Range is about 1000 km long and 300 km wide arcuate belt consisting of a series of imbricate thrust sheets with obduction of ophiolites emplaced onto southward (present coordinates) subducting continental Arctic Alaska terrane. The estimated 580 km of crustal shortening occurred in some parts of the Brooks Range (Mull, 1982; Nunn et al., 1987; Patton et al., 1994). Within the boundaries of National Petroleum Reserve Alaska (hereafter NPRA), the Colville basin covers a substantial portion and is abundant in geophysical datasets (Nunn et al., 1987). The northern boundary of the Colville basin is an Atlantic-type rifted continental margin (Grantz and May, 1982; Grantz et al., 1994) that extends into the shoreline of Alaska where a broad subsurface basement ridge, the Barrow Arch, developed during a rifting episode from Jurassic to Early Cretaceous. The basin extends offshore toward west under the Chukchi Sea into the northwestward-trending Herald Arch and the northward-trending Chukchi platform. These geological features are remnants of a late Paleozoic to Early Mesozoic south-facing Arctic continental margin. On the far east, the basin narrows down along the Alaska-Canada border (Bird, 2001).

2.2 Tectono-stratigraphic Sequences

The North Slope of Alaska is underlain with rocks as early as Late Proterozoic. Based on tectonic history, genetic relations and origin, the rocks of the North Slope of Alaska can be subdivided

stratigraphically into four primary sequences (Hubbard et al., 1987; Bird, 2001). The oldest sequence; Franklinian sequence, holds clue to complex geologic history due to deformation caused by Ellesmerian orogeny. This sequence mostly consists of Pre-Devonian deformed and metamorphosed basement complex (Grantz and May, 1982; Bird and Houseknecht, 2011). The basement complex is shallower near the Barrow Arch and is deepest at the northern edge of Brooks Range. Following the Ellesmerian orogeny, a regional unconformity developed and Ellesmerian sequence was deposited on the passive margin of Arctic shelf. This sequence from Mississippian to Triassic age consists of carbonate and clastic continental shelf deposits (Bird, 2001). Beaufortian Sequence of Jurassic and early Cretaceous consists of syn-rift deposits characterized by stacked sequences of southward prograding clinoforms (Houseknecht and Bird, 2011, p. 34). A prominent feature in this sequence is the break-up unconformity, also known as the Lower Cretaceous Unconformity (LCU), at the crest of the Beaufortian sequence. On a regional scale this unconformity truncates the reservoir and seal rocks near the Barrow Arch and hence plays a vital role in the oil and gas accumulations. More importantly, LCU defines the base of the oncoming clastic sediments of the Colville basin which is important for constraining the geometry of Colville basin for flexural studies. Beaufortian is the last sequence which has the northerly source of sediments. The Brookian sequence are derived from the south as a result of the collisional orogeny of the Brooks Range and comprises of progradation cycles characterizing dramatic sea level rises and substantial shifts of paleo shoreline (Bird, 2001; Decker, 2007). Thick clastic sediments, above 7620m (25,000 ft), are deposited into the Colville basin (Houseknecht et al., 2009).

2.3 Geometry of Colville Foreland Basin

Colville basin is about 200 km wide with maximum depths of 8 km adjacent to the Brooks Range toward its southern edge. A complete stratigraphic column of Colville basin is shown in (Figure 5). The basin extends laterally from west to east spanning about 650 km area. The structural style of the basin is a tapered wedge (Figure 6) that shallows up-dip towards its northern edge close to Barrow Arch, where the depth of the basin drops to 500 m. By investigating the seismic data, presence of massive prograding clinoforms sequences in the Nanushuk and Torok formations can be identified, indicating a high rate of sediment influx and presence of large accommodation space in the Colville basin. This observation is also supported by the structural map of LCU, which shows a structural relief of 8 km deep basin for clastic volume shed from the Brooks Range.

The seismic interpretation of frontal Brooks Range and North Slope of Alaska shows evidence of significant detachment surfaces that developed during the Tertiary deformation phase affecting the southernmost part of the foredeep (Mull, 1982). The Kingak formation, which lies below LCU (Figure 5), separates foreland sediments from the passive shelf margin acting as a surface for thrust fault propagation and structural relief (Moore et al., 1994; Stier et al., 2014). Northward tectonic transport of Early Brookian fold and thrust belt is evident in the southern part of the Colville basin, which ceased possibly by Aptian (Mull, 1982; Moore and Box, 2016).

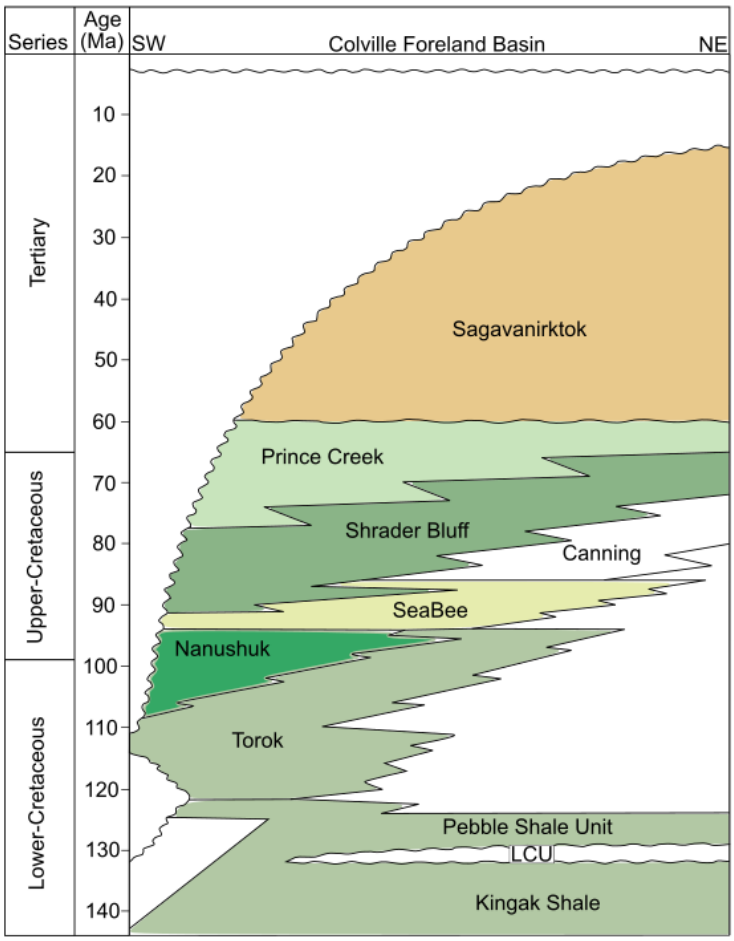

Figure 5. A stratigraphic column of Colville basin. The Kingak shale constitutes the uppermost formation of passive shelf margin. The Lower Cretaceous Unconformity LCU is the regional unconformity separating Colville basin deposits from the passive margin.

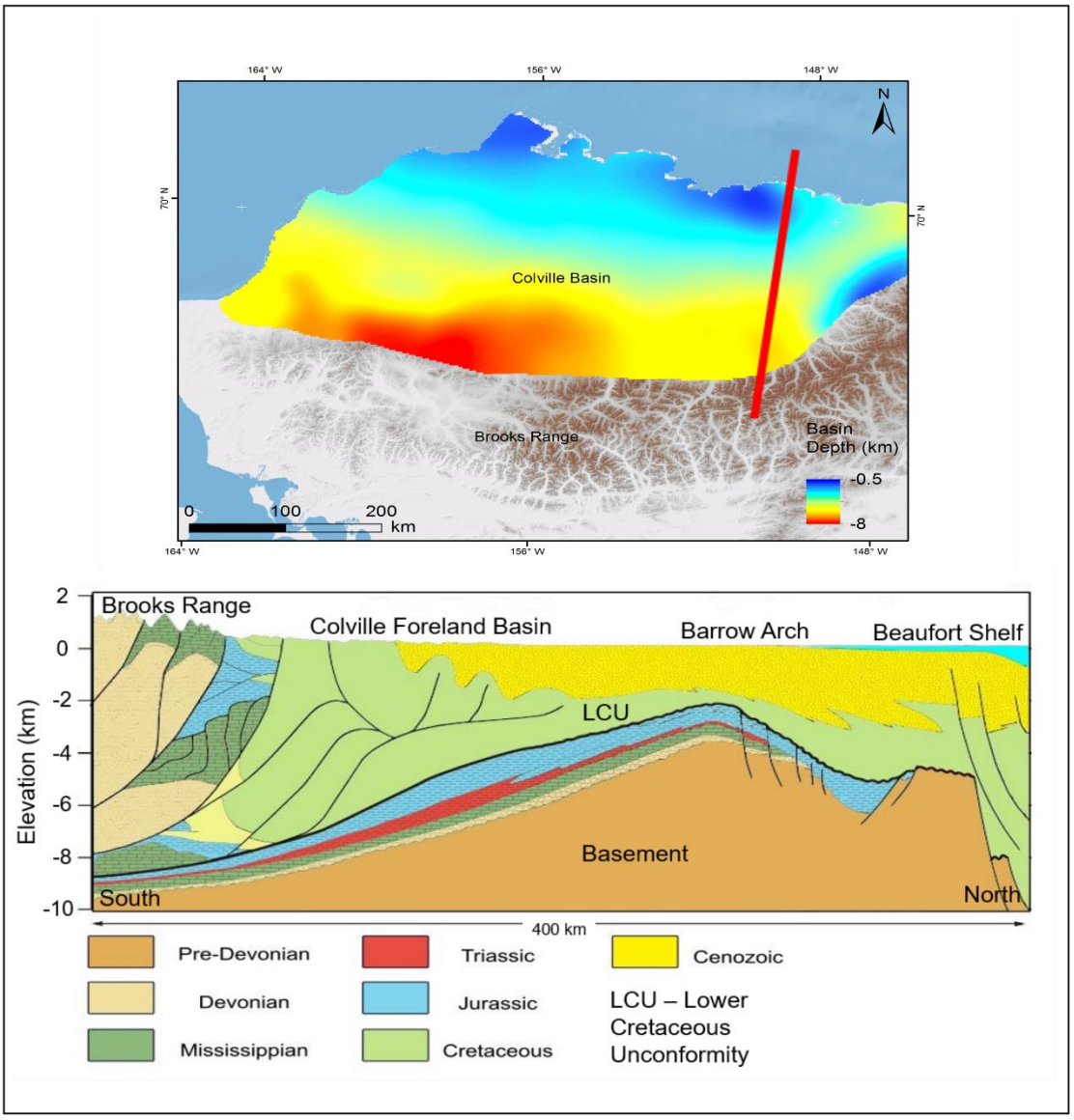

Figure 6. A south to north cross-section from northern Alaska showing age distribution of rocks. The basement is mainly composed of Pre-Devonian rock. The black line shows the LCU separating passive margin deposits from orogenic sediments. Colville basin comprises of mainly Cretaceous and Cenozoic rocks. Towards north, the LCU decreases in depth close to Barrow Arch due to uplifting of this basement ridge.

2.4 Crustal Structure of Northern Alaska

Crustal architecture of continents is often studied by methods such as seismic tomographic imaging with active source experiments for e.g., S and P seismic receiver functions. In general, the Alaska continent shows strong variability of crustal thickness because of variations in topography, multiple episodes of terrane accretion, and influence of orogenic activity. Southern Alaska shows high variability of crustal thickness and more than 55 km crustal thickness is observed near the Pacific margin whereas the central Alaska is average 32 km deep (Fuis et al., 2008). South and south-central Alaska is extensively imaged by seismic broadband due to active subduction of Pacific plate under the Alaska (Miller et al., 2018). But on the other hand, northern Alaska, due to quiescence in recent tectonic activity, has been sparsely imagined as a result of limited availability of data.

Trans-Alaska-Crustal-Transect (TACT) was the first experiment to image the deep crust of Brooks Range by using seismic reflection and refraction methods. TACT originally covered an extensive profile from the south to north 1350 km long covering entire Alaska (Fuis et al., 2008). In the northern Alaska segment of TACT, the profile spanned from coastal plains of Alaska through the Brooks Range. This study identified an asymmetrical crustal root beneath the Brooks Range with maximum thickness of the crust to be 46 km.

Crustal evolution of northern Alaska is also defined by 3D modeling of Bouguer anomalies carried out by (Torne et al., 2020) that shows prominent regional lows ranging from -140 to -60 mGal in the mountainous regions of the Brooks Range (Figure 7). This regional low trend extends further

north, towards the Colville foreland basin where Bouguer anomalies ranges from -60 to -20 mGal (Figure 7). The overall trend of regionally low gravity anomalies highlights crustal thickening beneath the Brooks Range. Towards the north of the Colville basin, the gravity anomalies abruptly change from low to high values. The observed Bouguer anomalies near the shelf reaches to 180 mGal. This is attributed to the thinner crust of the Beaufort shelf that formed due to the rifting of the Canada basin.

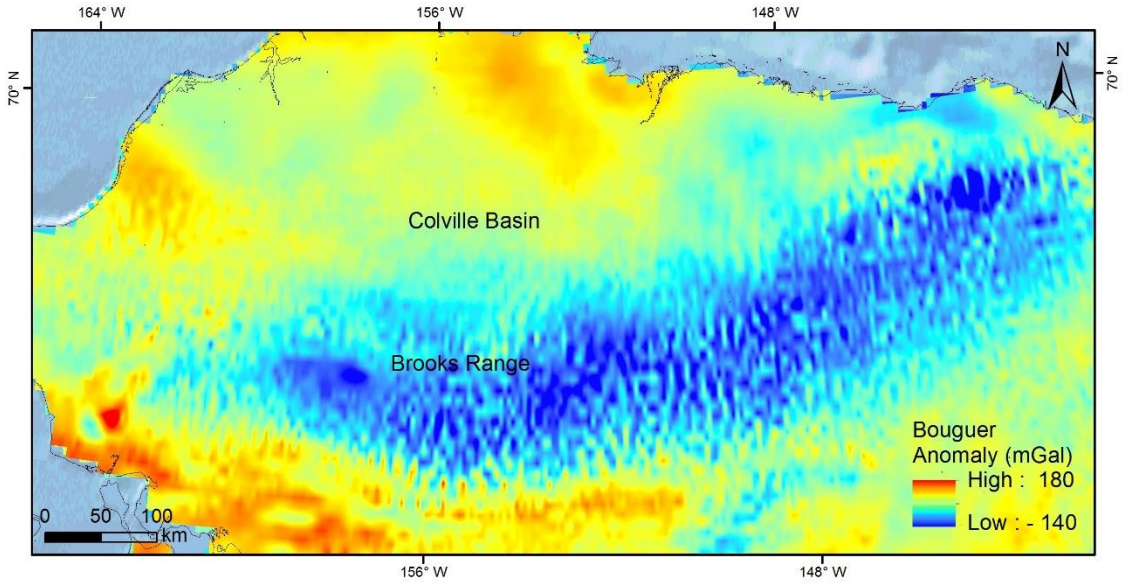

Figure 7. Bouguer anomaly map showing crustal thickening of the crust beneath the Brooks Range and the Colville foreland basin.

CHAPTER 3

FLEXURE MODELING OF NORTHERN ALASKA

3.1 Definition of Foreland Basin

Foreland basins are formed parallel to the orogenic belts. They are formed due to immense mass created by the crustal thickening associated with the evolution of orogenic belts causing the lithosphere to bend by a process known as the lithospheric flexure (DeCelles and Giles, 1996; DeCelles, 2012) . This flexure causes the sediment thickness in the basin to decrease away from the thrust sheets. The shape of a foreland basin is controlled by the strength and rheology of the lithosphere. The sediments form a characteristic wedge-shaped sequence and provides an important record of the timing, paleogeography, and subsidence history of the basin as it grows and migrates outwards during the orogenic convergence (Kearey et al., 2009).

3.2 Strength of Lithospheric Plate

The parameter that characterizes the strength of the lithosphere is called the flexural rigidity (D) which is the resistance to bending under the applied loads. In other words, it can also be defined in terms of the elastic thickness (Te) of the lithosphere. The lithosphere acts as an elastic plate under the applied loads and maintains gravitational equilibrium over the geologic time. The relationship of the elastic thickness with the thermal age is relatively simple, in the oceanic lithosphere the elastic thickness increases with the age of the oceanic crust (McKenzie and Fairhead, 1997). In the oceanic regions, the elastic thickness estimated from the gravity field generally corresponds to a depth of the 450° C isotherm. However, there is no direct relationship

of the elastic thickness with the thermal age for the continental crust (Burov and Diament, 1996; Brown and Phillips, 2000) . Instead the variations in the elastic thickness are caused by the prolong history of complex tectonics.

The elastic thickness of the lithosphere depends on many factors; such as composition and density structure, stresses and thermal states, and the geometry and mechanical properties of the lithosphere (Burov and Diament, 1995; Lowry and Smith, 1995). Significant spatial variations occur in the strength of the continental lithosphere. Usually the strength increases in the Precambrian and the Archean cratonic regions, whereas the Phanerozoic lithosphere is usually weaker. In general, the elastic thickness does not correspond to a physical depth, but rather represents the integrated brittle, elastic and ductile strength of the lithosphere. Although the elastic thickness does not represent an actual depth to the base of the mechanical lithosphere, its spatial variations reflect relative lateral variations in the lithospheric mechanical thickness (Pérez-Gussinyé et al., 2009). Te (elastic thickness) and D (flexural rigidity) for an elastic plate can be related by a simple equation.

$$Te = \sqrt[3]{\frac{12(1-\sigma^2)D}{E}}$$

where the elastic constants E and σ are Young's modulus and Poisson's ratio.

The knowledge of strength distribution contributes to a better understanding of mechanisms behind deforming processes, such as rifting, orogenesis, isostasy, postglacial rebound, origin and evolution of sedimentary basins, seismicity, and volcanism (Eshagh et al., 2020).

3.3 Flexure Model Description

The elastic parameters of a flexed lithosphere can be derived using several modeling techniques. In the past, the relationship between the gravity and topography has been widely used to model the deflection of the lithosphere. More recently, a variety of 3D numerical modeling techniques have been used by experts to investigate the flexural bending and the deflection parameters. Of these, the most common methods are the Finite-element method and the 3D analytical solutions.

To calculate the flexure of the bending plate underneath the North Slope of Alaska, an assumption is made that defines an elastic plate inviscid over a dense asthenosphere that is in isostatic equilibrium. The plate is flexed downward in response to the topographic load, with contributions from the adjacent sediment-filled foreland basin and the crustal root (Figure 8). The downward flexure is also accompanied by an additional force; called the hydrostatic restoring force, caused by the replacement of mantle rocks by the lighter density crustal rocks. The crust beneath the load is effectively thickened by the amount by which the Moho is depressed. For this study, it is assumed that the region of deflected Moho as a result of flexure of basin is filled with the density of air. To calculate the restoring force, density contrast between the Moho boundary and the crustal root is used. The calculated restoring force is given by.

$$\Delta\rho = \rho_{mantle} - \rho_{crust}$$

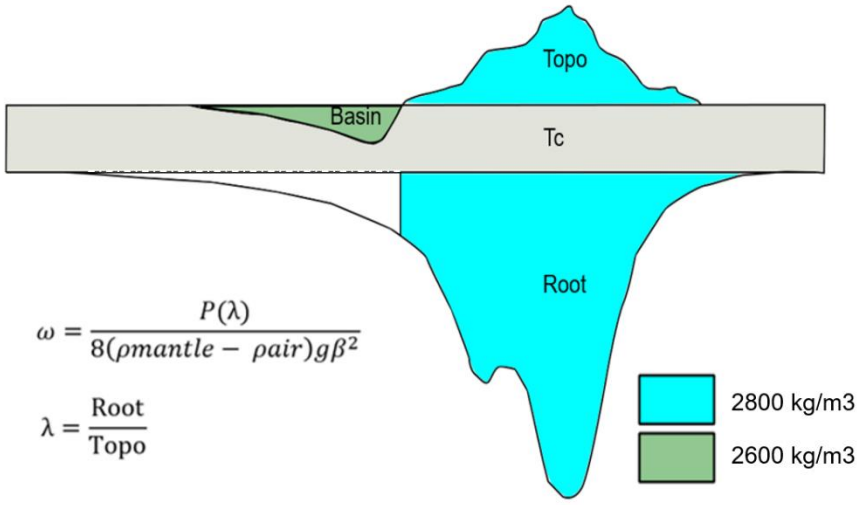

Figure 8. The conceptual model shows that the applied load is calculated from the excess thickness of the crust (topography and crustal root) and basin load colored in blue. The equation calculates flexural parameters where Tc: thickness of un-deformed lithosphere, ω: max deflection, P: topographic load, $\rho mantle$: density of mantle, ρair: density of air, g: gravity acceleration, β: flexural parameter and λ is the ratio between the thickness of crustal root and topographic height (adopted from Pirouz et al., 2017).

The modeling approach is based on analytical solutions derived from solving partial differential equations that are stable in irregular topography with a high spatial resolution and accounts for all the parameters associated with the deflection of plate (e.g. Wienecke et al., 2007). According to this method, the flexure (ω) of a thin elastic plate is calculated by following three distinct solutions:

$$1.\ \omega = \frac{P}{8(\rho mantle - \rho crust)g\beta^2}$$

$$2.\ \omega(x,y) = \frac{P}{2\pi\beta^2(\rho mantle - \rho crust)g} \times \left\{ \begin{array}{c} \frac{(r_{x,y})^2}{2^2} \times ln(r_{x,y}) - \frac{(r_{x,y})^6}{2^2.4^2.6^2} \times \left(ln(r_{x,y}) - \frac{5}{6} \right) + \cdots \\ + \frac{\pi}{4} \left(1 - \frac{(r_{x,y})^2}{2^2.4^2} + \frac{(r_{x,y})^8}{2^2.4^2.6^2.8^2} \right) \\ \ldots - 1.1159 \times \left(\frac{(r_{x,y})^2}{2^2} - \frac{(r_{x,y})^6}{2^2.4^2.6^2} + \cdots \right) \end{array} \right\}$$

$$3.\ \omega(x,y) = \frac{P}{2\pi\beta^2(\rho mantle - \rho crust)g} \times \sqrt{\frac{\pi}{2}} \frac{e^{-(x,y)\sqrt{1/2}}}{\sqrt{(r_{x,y})}}$$

$$\times \left\{ sin\left[(r_{x,y}) \sqrt{\frac{1}{2} + \frac{\pi}{8}} \right] - \frac{1}{8(r_{x,y})} sin\left[(r_{x,y}) \sqrt{\frac{1}{2} + \frac{3\pi}{8}} \right] + \cdots \right\}$$

Here β is the flexural parameter, P is the applied load and $r_{x,y}$ is the radial distance from the point of origin. The first solution calculates the maximum depth of deflection; the second solution accounts for log-function where $r_{x,y} \leq 2\beta$ and the third solution accounts for sine-function where $r_{x,y} \geq 2\beta$. The log-function is only valid for small values of the radius $r_{x,y}$, whereas the deflection values produced by the sine-function are underestimated for smaller values of the radius $r_{x,y}$. The analytical solution is derived by using all three methods by using the expression $r_{x,y} = 2\beta$ for the change in the function from log to sine. To consider point load distribution, the Green's function is used which is simply given by dividing P by the ω. The Green's function for a point load represents a two-dimensional (2-D) radial cross section in the *r*-*z* plane (*r* is the radial coordinate position) across a radially symmetric flexural basin, normalized by the magnitude of the load. By convolving the Green's function with P, the deflection due to the distributed loads can be calculated.

3.4 Available Data

In order to model the flexure of the Colville basin, first the geometry of the basin is constrained. The base of the Colville basin is highlighted by a regional unconformity known as the Lower Cretaceous Unconformity (LCU) which separates the underlying passive shelf margin from the overlying orogenic sediments shed from the Brooks Range. To obtain the geographical extent of the basin, a database has been created using the Petrel software that includes subsurface seismic and wellbore data (Figure 9) provided by the United States Geological Survey (USGS), and a published structural map of LCU adopted from (Bird and Houseknecht, 2011). Data available from USGS is vintage seismic data acquired in 1980s and therefore does not offer good quality seismic profiles. This causes challenges in the seismic interpretation. There are several wellbores available in the NPRA from which 4 wells (Tunalik, Peard, Inigok and North-Inigok) are used for seismic to well tie analysis. Using the velocity surveys, a time to depth relationship is established for the survey area and the formation tops are picked on major seismic profiles. The target horizon; LCU, was then interpreted on the seismic data, interpolated into a surface, and finally converted from time to depth domain. The final structural map obtained from the seismic interpretation highlighting the geometry of the Colville basin. Similarly, the published LCU map was georeferenced and digitized using ArcGIS software and imported into Petrel as a surface.

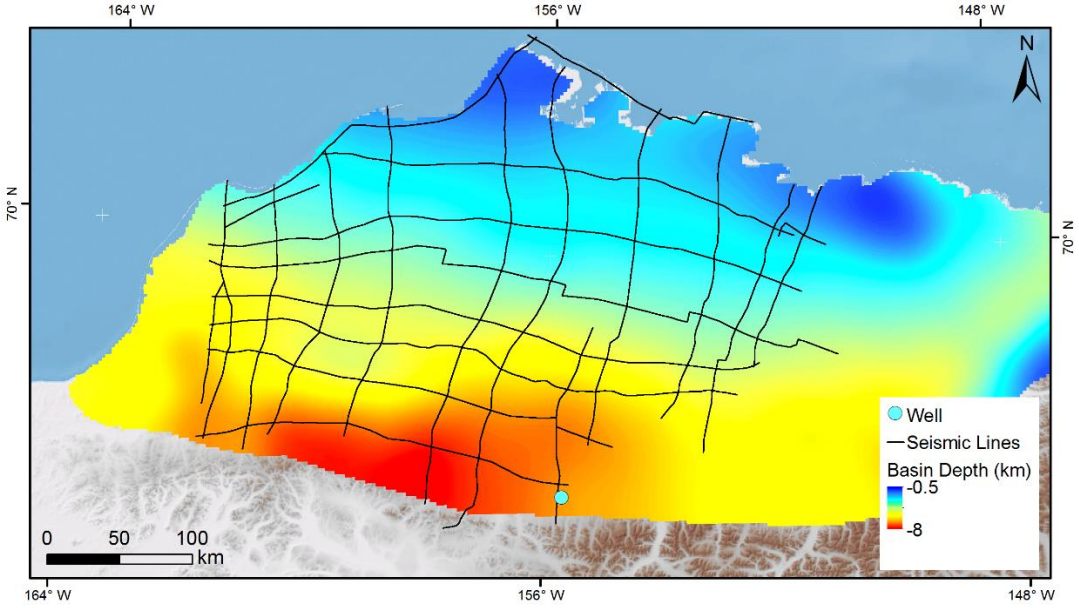

Figure 9. Display of 2D seismic lines available from USGS and a colored structural map of base of the foreland defined by regional unconformity; LCU. Data source (USGS and Houseknecht and Bird, 2011). The blue circle shows the location of borehole data used to estimate vertical density variations in the Colville basin.

The resulting surface from seismic interpretation shows good correlation (Figure 10) with the published LCU map; however, the extent of LCU is limited in deeper parts of the basin where folding and thrusting affect seismic quality. The complete structural extent of the foreland basin is more thoroughly mapped in the published LCU. Furthermore, it has better quality seismic data processed with modern processing techniques and robust depth conversion, therefore providing the regional extent of the Colville basin. Hence, the LCU surface obtained from (Bird and Houseknecht, 2011) is used for the modeling purpose.

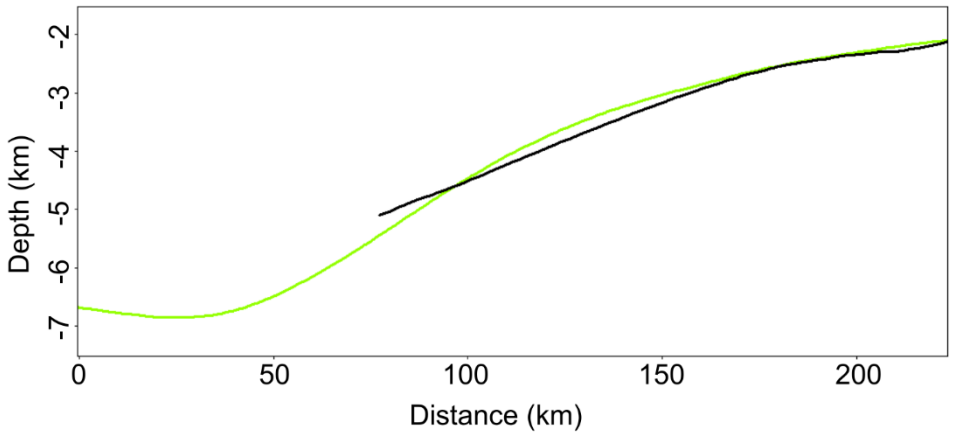

Figure 10. Cross-section of LCU correlation with published and interpreted structural surface of base of foreland. The results of seismic interpretation of LCU (black) correlates well in the shallower part of basin. In contrast, the published LCU (green) offers a geographical extent and a maximum depth of the Colville basin. The location of the cross-section is shown in Figure 13 section-B.

The depression in the bending plate occurs in response to sediment infill and adjacent topography. The amount of these loads accounts for a small fraction of total loads acting on the deflected plate (Beaumont, 1981). In general, the topographic load is proportional to the buried foreland sediments. This relationship is significant for evaluating the elastic properties of a flexed lithosphere. To estimate the current topographic load, DEM (Digital Elevation Model) derived from (EDNA - Elevation Derivatives for National Applications by U.S. Geological Survey, 2005) has been used which provided high resolution 60×60 m raster elevation grid for the northern Alaska region. For flexural modeling purposes, the raster elevation grid is converted into point dataset that can be easily interpolated into a surface with desired spatial resolution. Using the 3D Spatial Analyst; Raster-To-Point conversion tool of ArcGIS software, the raster elevation grid for the northern Alaska region is converted into point dataset. This dataset is then imported into Petrel software where a topographic surface is interpolated with the spatial resolution of 500 m. The

resulting surface is also clipped to represent the complete extent and the total load posed by the Brooks Range and the Colville foreland basin.

The first compositional change in the subsurface occurs at the crust-mantle boundary also known as Moho discontinuity. At this boundary the compressional wave velocity rapidly increases to ~8 km/sec. This change in the velocity can also be explained in terms of density variation between the crust and mantle. The mantle material is much denser than the overlying crustal material of low density. We constrain the boundary of the Moho discontinuity from the seismological Moho data (Figure 2) of entire Alaska assembled by (Torne et al., 2020) and references therein. The dataset is available in ASCII format and can be readily interpolated into a surface with desired spatial resolution. Moho dataset is imported into Petrel and then interpolated into a surface with 500 m spatial resolution representing the crust-mantle boundary for the study area.

3.5 Modeling Workflow

The flexure modeling of the Colville foreland basin is performed in the following stages. First, the spatial extent of the present-day Colville foreland basin is constrained. Then the flexure of the lithosphere beneath the present-day foreland is used to determine (1) if a flexural model can accurately describe the geometry of the basin (2) the best-fit parameters (i.e., Te), and the influence of subsurface dynamic loads. The influence of subsurface dynamic loads acting on the northern Alaska lithosphere is tested by analyzing if the amount of load posed by the topography of Brooks Range and the sediment load of the Colville basin is enough to produce the similar deflection as observed in the present-day basin geometry. For this purpose, the base of the LCU is used to

delineate the geometry of the foreland deposits. The base map of the foreland also helps to calculate the weight of sediment load in the Colville basin.

For the purpose of flexural modeling of the Colville basin, a database of all the input surfaces is created using available interpolated surfaces of (1) the base of the Colville basin represented by LCU surface, (2) the topographic surface and (3) the root-mean-square (RMSE) area that represents the total area of error calculation. These surfaces are then converted into ASCII format representing the elevation and the depth values at their corresponding x and y geographic coordinates. The spatial resolution of all the surfaces is set to a constant 500 m. This is an important step because inconsistent resolution between the input surfaces can lead to miscalculations or error in the programming software. Numerical calculations are carried out in the MATLAB software that supports an extensive and time-consuming iterative calculation for all the input surfaces.

The bent lithosphere of the northern Alaska region has been influenced by the post-collisional thrust front propagation from the south and as well as the northerly rift related subsidence that caused the uplift of the Barrow Arch. Due to this tectonic activity, the base of the Colville basin is deformed up to some extent. To avoid discrepancies in the modeling results, exclusion of deformed regions is significant for the flexural modeling. In the flexure model of the Colville basin, regions of uplift and post-collisional deformation are appropriately modified and clipped, and the total modified area of the basin represents approx. 83,000 km^2 area. The deformed regions, two large antiforms (see Figure 13a), are ignored for comparison between the observed and the modeled foreland basin. Also, the northern and north eastern part of the basin that is excluded (Figure 13a), represents the areas affected by the rifting of the Canada passive margin specifically the Barrow

Arch. This basement high particularly affects the northern part of the Colville basin and as a result, structural relief of the base of the foreland abruptly changes between the high and low values. Including these regions would possibly derive overestimated or underestimated values of the elastic thickness, therefore, they are excluded from the flexural modeling.

The deflection at each point is calculated iteratively using the equations as described in the section 3.2 and the elastic parameters used in the calculation are summarized in the (Table 1). The flexure model is tested by changing the elastic properties between the crust and the mantle boundary. Three cases of density variations are tested, and the output parameters are summarized in (Table 2) in section 5.2. The model produces a hypothetical basin model, a prediction based on the input elastic parameters, which can be compared to the observed present-day deflection for the purpose of separating the independent variables influencing the deflection of the Colville basin. A range of models has been calculated by stepwise increasing the elastic thickness values between 1 to 50 km. Similarly, the tested λ ranges from 1 to 10 with a stepwise increase of 0.1. The iterative modeling approach is adopted to find the best fit between the observed and the predicted foreland depths by testing all possible solutions. The corresponding elastic thickness value at which the root-mean-square is minimum, is the best fit model. The output data from the calculations include a deflection model of the Colville basin and an RMSE plot. The deflection model is the predicted foreland surface derived from the flexure calculations. RMSE plot is an interpretive plot of the elastic thickness of the lithosphere versus the ratio of root to topography (λ) . The plot also includes an RMSE value for each iteration. The implications of the modeled results are described further in detail in the section 5.2.

Table 1. Summary of elastic paraments used in the calculation of the flexural model.

Constant	Symbol	Value	Units
Young's Modulus	E	1×10^{11}	Pa
Poisson's Ratio	σ	0.25	
Gravity Acceleration	g	9.81	m/sec^2
Mantle Density	$\rho mantle$	3300	kg/m^3
Crustal Density	$\rho crust$	2800	kg/m^3
Basin Density	$\rho basin$	2600	kg/m^3
Air Density	ρ_{air}	1020	kg/m^3

CHAPTER 4

GEOPHYSICAL MODELING OF NORTHERN ALASKA

4.1 Concept of Gravity Anomalies

The term gravity refers to the combined effect of the earth's rotation and gravitational attraction exerted on an object with some mass (Turcotte and Schubert, 2002). The magnitude of gravity depends on the latitude, topography of the surrounding region, earth tides and density variations due to anomalous density bodies in the subsurface. In this study the change in the magnitude of gravity due to the subsurface density variations is the most significant. In continents the thickening of the crust can be explained by its corresponding negative gravity anomalies. This phenomenon occurs due to the presence of positive anomalies of continents above the ocean that is hydrostatically compensated due to negative mass anomaly of the thicker continental crust. Topography and density variations in the crust leads to inhomogeneity in the surface gravity which can be referred to as the gravity anomalies.

The study of gravity field is significant for geodesy and geophysics. In geodesy, the shape of the earth is explained by a geoid surface which can be simply defined as a surface of equipotential lines. Using the gravity anomalies, the geodesist explains the shape of the earth. In the field of geophysics, the gravity anomalies are also helpful to investigate the distribution subsurface mass and density. Geological structures in crustal to upper mantle depths can be very well constrained with gravity anomalies (Bonvalot et al., 2012).

4.1.1 Bouguer Anomalies

The gravity anomaly at a given point that is corrected for the height at which it is measure is called the Bouguer Anomaly. The Bouguer correction accounts for the attraction of material between the station and datum. Influence of local short wavelength topography is effectively removed by the Bouguer correction; however, it is not affective in removing the influence of regional long wavelength topography.

At any given point on the Earth' surface, the Bouguer gravity can be calculated by.

$$\Delta gB = g_{Obs} - g_{Theor}$$

In this equation, g_{Obs} is the observed gravity at a point and g_{Theor} is the theoretical gravity computed from the reference earth model given by.

$$g_{theor} = g_{Obs} - \gamma o + \delta g_{FAA} - \delta g_{Topo} + \delta g_{ATM}$$

Here, γo is the normal gravity at a point on the reference ellipsoid surface. Theoretical gravity is computed by applying a height or free-air correction; δg_{FAA} , a topographic correction δg_{Topo} and the atmospheric correction δg_{ATM} (Bonvalot et al., 2012).

4.1.2 Free-air Anomalies

The gravity field varies inversely with the square of distance. It is, therefore, important to correct for changes in elevation between the stations to reduce the field readings to a datum surface. The free-air correction does not take account of the material between the station and the datum plane. It is added to the field reading when the station is above the datum plane and subtracted when below it. There are two contributions to the surface free-air gravity anomaly. Contribution from

topography and the geometry of the Moho boundary. The vertical deflection of the Moho is expected equal to the vertical deflection of the lithosphere because the Moho is assumed to be a compositional change embedded in the lithosphere.

Critical analysis of the correlation between the gravity and topography indicates that the isostatic displacement of the Moho boundary can be preserved even when the topography is removed (Turcotte and Schubert, 2002). For example, surface erosion reduces the topography over long-term geologic time i.e. the lithosphere was initially loaded with topography and subsequently eroded with time. In this case, the theoretically gravity anomalies should also be eliminated. However, it is important to note that even though changes in the lithospheric thickness might occur, the displacement of the Moho boundary is permanent.

4.1.3 Gravity Anomalies and Isostatic Compensation

The lithospheric deflection due to the load of the mountain is dependent on the scale of the mountain. For example, a large horizontal scale (for e.g., 1000 km) mountain load, deflects the lithosphere downward whereas small scale loads do not deflect the lithosphere. Because the crustal rocks are lighter than the mantle rocks, this results in a low density “root” for the mountain ranges with a large horizontal scale. The mass associated with the topography of the mountains is compensated at depth by the low-density root. Because the Bouguer gravity correction for topography does not account for the negative root, the anomalies over mountain ranges are strongly negative. Negative mass of the mountain root cancels the positive mass of the mountain in the long wavelength limit (Turcotte and Schubert, 2002).

4.2 Concept of Isostacy

The fundamental concept of plate tectonics is based on rigid lithosphere overlying weak asthenosphere (Watts, 1978). It can be defined as a gravitational balance of large blocks of earth's crust as if they are floating on a denser underlying asthenosphere (Watts, 2001). the concept of isostacy can very well explain the physical concepts of equilibrium attained between the crust and the mantle and the existence of varying topographic heights on the surface of earth. To explain how isostacy supports the weight of mountain on the earth surface, there were two popular ideas in mid-19th century.

In 1858 a mathematician; Henry Pratt presented a model for the equilibrium of the mountains on the surface of the earth. The Pratt hypothesis states that the density of root changes laterally but have equal mass. The Airy hypothesis of isostatic compensation assumes that the thickness of the crustal blocks of constant density varies such that the thicker parts of crust ride higher. For example, a mountain compensated by deep crustal roots (Figure 11). The crustal root can be described as a relatively light material projecting down into the mantle and thus isostatically balancing the topographically high areas such as the mountains.

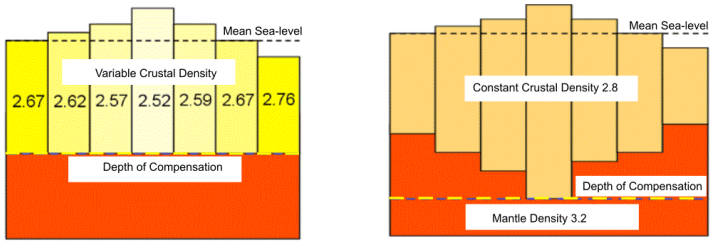

Figure 11. Pratt and Airy isostatic compensation schematic model. In Pratt isostacy, the density changes laterally and the material has equal weight at the depth of compensation. In Airy model the crustal density is constant, and the density contrast occurs below depth of compensation. Modified from (Beniest, 2018)

4.3 Elastic Thickness from Gravity Data

Analysis of gravity anomalies has been used in many studies of lithospheric flexure. Subsurface gravity anomalies arising due to density variations can be used to study the isostatic balance of mountains on the earth surface. There are two methods typically used to estimate the elastic thickness of the lithosphere with the gravity data (Watts, 2001). The forward modeling, a relatively simple approach, considers known load structures, for e.g. a sedimentary basin or a seamount, and estimates the elastic thickness based on the trial and error method. On the other hand, the inverse method uses the relationship between the observed gravity and topography data in the spatial frequency (wavenumber) domain, namely the admittance and the coherence. The observed measures are subsequently inverted against the predictions of the elastic plate models, giving estimates of Te and other lithospheric parameters (Forsyth, 1985; Eshagh et al., 2020). The estimates of elastic thickness from the cross-spectral analysis are often over or under-estimated (McKenzie, 2010).

4.4 Available Data

In this study, the free-air gravity anomalies for the northern Alaska region has been used as a primary input dataset for the purpose of geophysical modeling. A high resolution gravity anomaly grid; World Gravity Map (WGM2012), free-air surface gravity anomaly grid is available from (Bonvalot et al., 2012). WGM constitutes a set of gravity anomaly maps and digital grids computed at global scale from available reference Earth's gravity and the elevation models. The surface free-air anomaly dataset is derived from EGM2008 Geopotential model and the ETOPO1 Global Relief Model. This is a comprehensive free-air anomaly dataset that considers the contribution of most

surface masses (atmosphere, land, ocean, inland seas, lakes, ice caps and ice shelves) and the computations are based on accurate geodetic and geophysical definitions of gravity anomalies. The anomaly grid is computed with a $1' \times 1'$ resolution and the reference density used for the Bouguer and isostatic anomaly is 2670 km/m^3. For this study, the grid is imported into Petrel and interpolated into a surface with spatial resolution of 500 m.

4.5 Modeling Workflow

The relationship of gravity anomalies and topographic data have been used in many flexural studies. Previously (Watts and Burov, 2003) suggested that to verify estimates of elastic thickness one can compare results of forward modeling of geological observation with spectral analysis of gravity and topography data. In the latter method elastic thickness of the lithosphere is directly derived from gravity and topography data. In this study the geophysical investigation is conducted to support the flexural model results of direct geological observations with the geophysical investigations conducted through the gravity anomalies. However, here the geophysical calculations does not include calculation of elastic thickness of the lithosphere, instead, free-air surface gravity anomalies are calculated from the flexure model and compared to the observed free-air anomalies available from (Bonvalot et al., 2012). Similarly, free-air surface anomalies are also calculated from the available Moho boundary data (Torne et al., 2020) and compared to observed and flexure calculated free-air anomalies.

First, FAA obtained from the WGM2012 is considered as an observed gravity anomaly dataset for the study area. The principle source of density variations in the subsurface is from the crust/mantle boundary and concluded to be the source of measured gravity anomalies. To calculate Bouguer

anomalies and Free-air Anomalies (FAA) from the flexure modeling results, following equations are considered.

$$\Delta g_{(x,y)} = 0.0419(\rho_c - \rho_m)(Moho_{(x,y)} - T_c)$$

$$\delta gB_{(x,y)} = 0.0419\left[(\rho_c - \rho_{air})\left(Topo_{(x,y)} - T_c\right) + (\rho_b - \rho_c)\left(Basin_{(x,y)}\right)\right]$$

$$\Delta g_{elev_{(x,y)}} = \Delta g_{(x,y)} + \delta gB_{(x,y)}$$

Here equation 1 2 and 3 calculates Bouguer anomaly ($\Delta g_{(x,y)}$), Bouguer Correction ($\delta gB_{(x,y)}$) and Free-air Anomaly ($\Delta g_{elev_{(x,y)}}$), where ρ_b, ρ_c and ρ_m are basin, crust and mantle density, respectively. The depth of basin and Moho is given by $Basin_{(x,y)}$ and $Moho_{(x,y)}$, topography is $Topo_{(x,y)}$, and undeformed crustal thickness is given by T_c (Pirouz et.al., 2017 and reference therein).

The density values are extracted from the available deepest wellbore in the NPRA (Figure 9) to identify the vertical density changes in the Colville basin. The investigation of wellbore density data indicates that the density increases as an average from 2300 kg/m^3 to 2600 kg/m^3 at the deepest part of the basin (Figure 12).

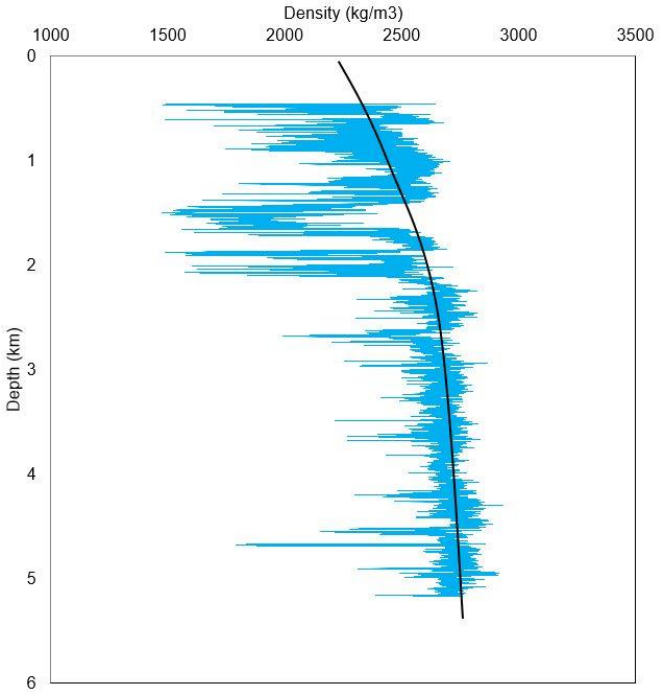

Figure 12. Vertical density variation with increasing depth in the Colville basin. The blue curve represents the measured density in the borehole. The well is located at the southernmost edge of the Colville foredeep. See the blue circle in Figure 8 for the exact location. The black curve corresponds to a polynomial function that averages the depth distribution of density.

The calculated anomalies are derived with two methods. The first method includes prediction of free-air surface anomalies (FAA) with the deflection model of Colville foreland basin. In this method, the FAA is calculated using the equations given in this section. For the calculation of anomalies, density parameters given in (Table 2) in section 5.2 are constrained that accounts for variation in crustal and basin densities. Similarly, topographic height is constrained by an interpolated surface of topography representing elevation of mountain above mean sea level. The surface that represents flexural model of Colville basin constrains the basin depth. Both model and topographic surfaces are gridded with spatial resolution of 500 m and the anomalies are calculated only for specified area where all dataset is available. On the other hand, the second method includes

calculation of the free-air anomalies with available Moho data from (Torne et al., 2020). In this method, the undeformed crustal thickness is estimated to be 37 km. First the Bouguer anomaly is calculated by subtracting undeformed crustal thickness from the Moho depth. Here the Moho depth is constrained by an interpolated surface with 500 m grid spacing. In the next step, Bouguer correction is calculated and finally the free-air anomalies are calculated by adding Bouguer anomaly to the Bouguer correction. All the calculations are carried out in Petrel software using the "Calculations" toolbox of interpolated surfaces.

CHAPTER 5

RESULTS AND DISCUSSION

5.1 Flexure of Colville Basin

Flexural modeling very well constructs the modeled deflection of the Colville basin which is illustrated in the (Figure 13), where observed A and modeled B foreland geometry is shown. The total area of observed foreland basin used for the model is approx. 83,000 km^2. Section 3.5 has a detailed account on the significance of cropping out antiforms in the observed map. Overall, there is an excellent correlation between the observed and modeled foreland geometry with some systematic misfit that is further described next.

Three cross-sections A, B and C obtained from the modeled area describes the misfit observed in the flexural model (Figure 14). Section A is the region least affected by post-collisional deformation, and hence the overall geometry of predicted and observed foreland depths shows an excellent fit. Section B covers the full width of the basin and has a remarkable correlation between observed and predicted deflection. However, there is slight misfit in the northern part of the basin where the model predicts shallower depths of the foreland, this misfit could be due uplifting effects of the Barrow Arch basement high. Section C is shown in the most deformed region (for e.g., see large antiform; Figure 14a) of the basin and a mismatch between the observed and predicted foreland deflection is evident in the deepest part of the basin (Figure 14c). The deepest part of the basin is where the post-collisional deformation most affected the base of the Colville basin. In this region, the model predicts shallower depths as compared to the observed depth. Since an excellent correlation exist between the observed and modeled foreland geometry, it can be inferred that the

load posed by the Brooks Range and sediments of the Colville basin is able to deflect the northern Alaska lithosphere and produce a similar deflection as observed in the Colville basin.

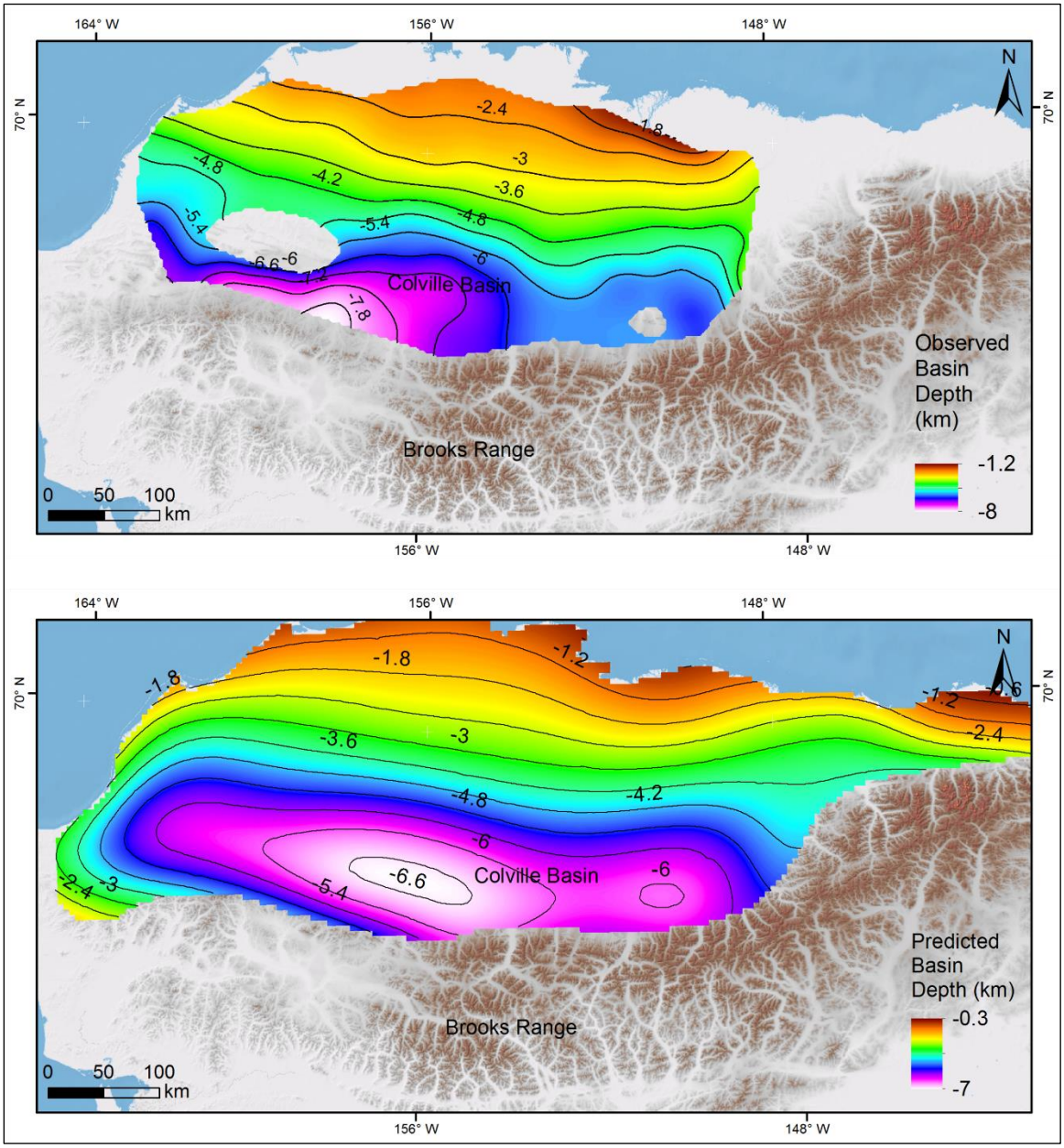

Figure 13. Observed (a) and best model predicted depth (b) of the base of foreland sediments of the Colville basin. The area excluded in the calculation of RMSE is shown in (a).

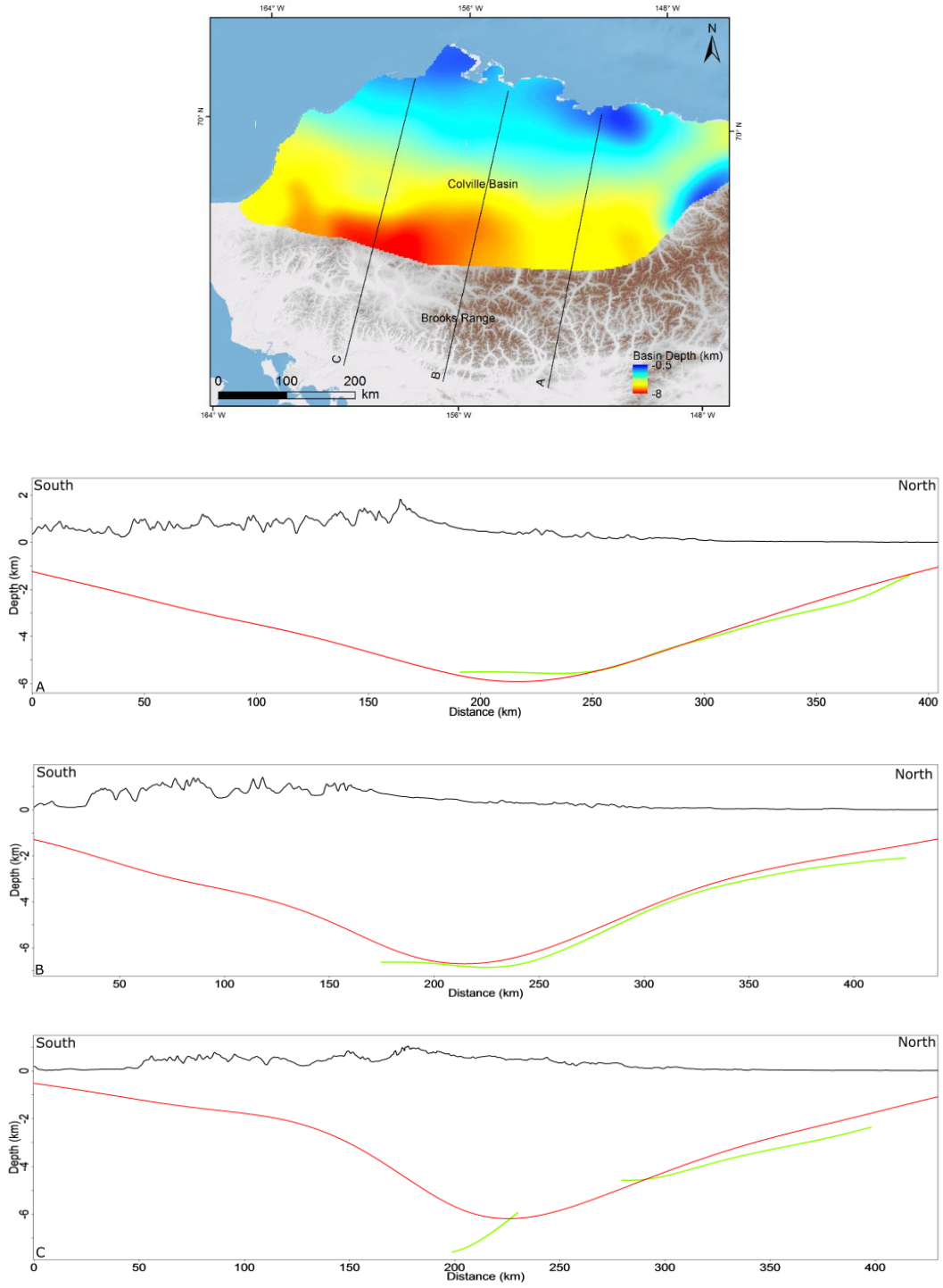

Figure 14. Cross-sections (A B and C) in the study area showing observed and predicted flexure of the Colville basin. The green line represents the observed depth to the LCU, and the red line represents the modeled depth to the LCU. Location of sections shown in the inset map above.

5.2 Elastic Thickness (Te)

Based on the weight of the Colville basin and the Brooks Range, the best fit model calculates the maximum elastic thickness of the lithosphere beneath the North Slope to be 16 km. The misfit error (RMSE) between the observed and predicted foreland depth is lowest when density contrast between the crust and mantle ($\Delta\rho$) is minimum (Table 2). However, with these parameters, the corresponding elastic thickness (13 km) seems under-estimated. The optimal solution accounts for $\Delta\rho$ to be 500 kg/m3 where mantle density is 3300 kg/m^3 and crustal density is 2800 kg/m^3, provide a more realistic root/topo ratio of 4.5, reasonable RMSE value of 225 m, and obtained elastic thickness of 16 km (Figure 15). These parameters best describe the observed and predicted foreland depths of the Colville basin.

Table 2. Summary of modeling results. Elastic thickness, RMSE of Deflection models, Root to topography ratio and crust-mantle density variations are listed below for three models.

Te (km)	Deflection RMSE (m)	Root/Topo Ratio (λ)	Density Variation $\Delta\rho(kg/m^3)$
16	252	4.5	500
14	225	3.9	400
13	205	3.4	300

One implication of the flexure model is that the lithosphere beneath the North Slope of Alaska has low elastic strength. Calculated 16 km elastic thickness suggests that the lithosphere is not able to transmit bending stresses deeper in the crust. In general, a weak lithosphere is also young and hot. However, it is also possible that the foreland basins may inherit the low elastic thickness values as they migrate over a passive margin and remain low for long durations (Watts, 1992). In northern Alaska, it is possible that during the collision of Arctic Alaska terrane with the oceanic arc, the

lithosphere inherited the low elastic thickness and has considerably remained low after collisional tectonics ended.

The elastic thickness computed for the northern Alaska is low when compared to other foreland basins such as Appalachians and Zagros. However, it is within the range of previous values determined at Aquitaine and west Taiwan foreland basins. Comparison between Colville basin's wavelength with modern systems like Zagros and Taiwan shows validating results of lithospheric elastic thickness estimation. The Zagros foreland basin width is approximately 450 km and elastic thickness about 50 km. In the Taiwan foreland basin, basin width is 110 km and elastic thickness is 13 km (Lin and Watts, 2002, Pirouz et al., 2017). Considering these observations, obtained 16 km elastic thickness with 200 km basin width for the Colville basin seems reasonable as compared to the other foreland basins.

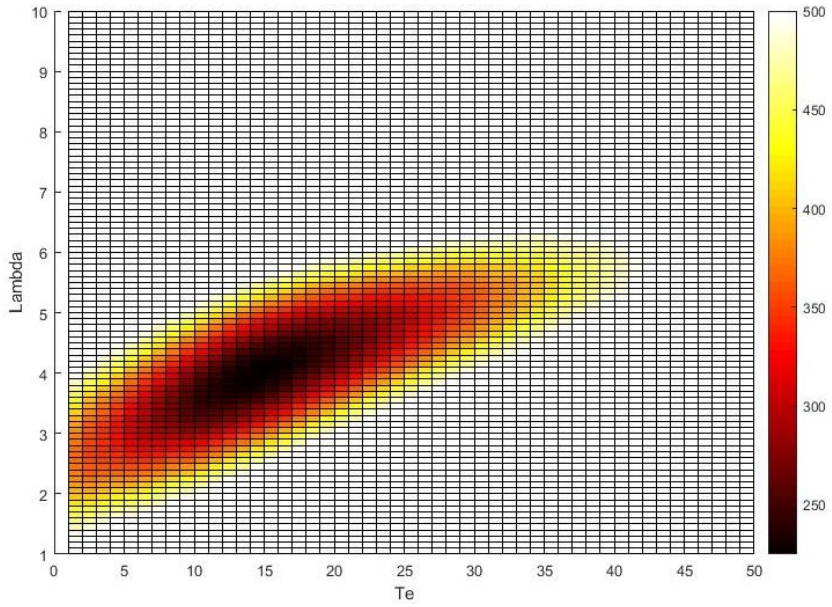

Figure 15. Root Mean Square Error (RMSE) between modeled and observed foreland depths as a function of the elastic thickness (Te) and the scaling factor between root and topography (λ).

5.3 Implication for Subsurface Loads

The results of this model indicate that static loads associated with topography and sediment infill and the subsurface load of crustal root well explain the flexure of the lithosphere beneath northern Alaska. The model yields an excellent fit of observed and predicted foreland depths that covers significant area (83,000 km^2) of the Colville basin. This implies an additional subsurface dynamic load is not required in the northern Alaska region to deflect the downward bending plate. The modeling results also shows contrasting results compared with the previous study led by Nunn et al., 1987. There are several possibilities, the most obvious one is that they used a simple 2D modeling approach and assumed that the geometry of Colville basin is relatively uniform. However, a detailed analysis of geometry reveals that the depth of the Colville basin varies abruptly adjacent to the Brooks Range as seen in the (Figure 13a). It can be concluded that the geometry is not uniform in the Colville basin. A more robust 3D modeling technique that accounts for geometrical variations in the basin was needed to accurately describe the observed flexure of the Colville basin.

Flexure results that estimated high values of elastic thickness predicted by Nunn et al., 1987 assumed a considerable force exerted by the downward subducted plate. For a high value of elastic thickness to hold true, it means that the mantle must transmit a huge amount of force to produce the observed flexure of the Colville basin. It has been established that the elastic strength of the lithosphere dissipates at the crust-mantle boundary with exceptions to the cratonic regions (Maggi et al., 2000). Therefore, it is not suitable to invoke an additional subsurface force that would cause the deflection of the Colville basin in the case of northern Alaska. It is likely that the initial results

that assumed no additional subsurface load (Nunn et al., 1987; Figures 4 and 5), creates a mismatch between the observed and predicted foreland depth as a result of their assumption of a uniform foreland geometry of the Colville basin. Furthermore, they considered the base of the foreland as a stratigraphic interval known as the Pebble Shale Unit which is considerably shallower than the break-up unconformity; LCU, that has been used to define the base of the Colville basin in this study. Therefore, 3D flexure model used in this study accurately predicted the observed foreland depth in the Colville basin.

5.4 Gravity and Flexural Support

The results of the geophysical investigation indicate that the predicted free-air anomalies from flexural model better defines the gravity anomalies of Colville basin and as well as the Brooks Range. In (Figure 16) results of observed and calculated anomalies are shown as color map where anomalies ranges from -50 – 150 mGal. The highest values are characterized by red color and the lowest values are shown with blue. The predicted (Figure 16a) shows excellent correlation with observed (Figure 16b) free-air anomalies. The overall trend shows that the Brooks Range is characterized by a belt of yellowish to red trend. These anomalies indicate that the crust beneath the Brooks Range is thicker as compared to adjacent foreland area where values of anomalies decreases to about -50 mGal.

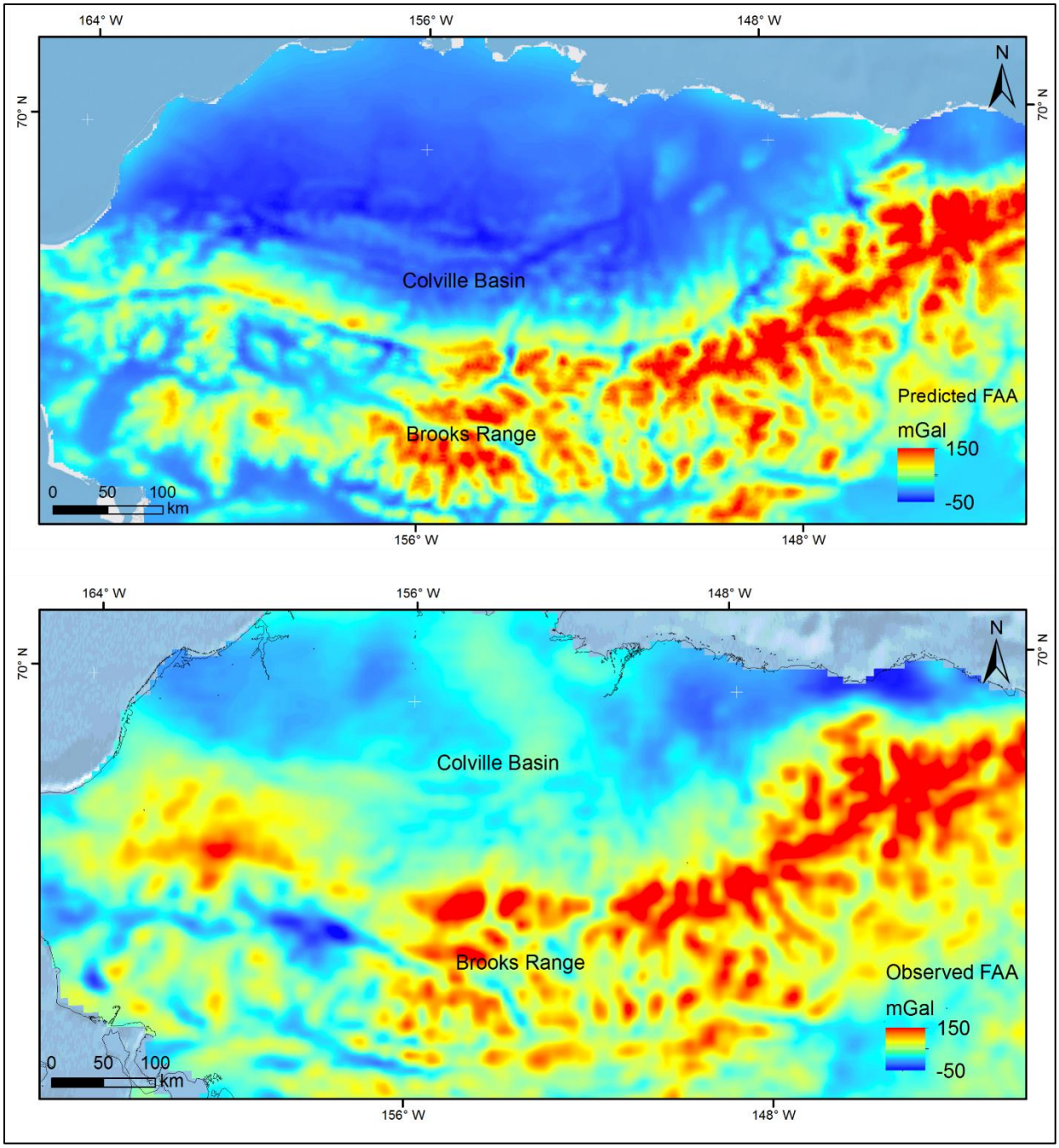

Figure 16. Upper part (predicted from flexure model) and lower part (observed) free-air anomalies (FAA). Brooks Range is characterized by particularly closer to zero anomalies (yellow) in the main thrust belt except for high values (red) where the belt extends further into the present-day shelf. Colville basin has typical foreland basin low anomaly response (blue color).

To further examine the calculations three south-to-north cross-sections are shown in (Figure 17) that spans 400 km in length and covers full extent of study area. The black curve represents observed anomalies and red curve represents the predicted anomalies. The northern part of the cross-sections shows very well fit between observed and predicted curves. This region that spans about 200 km in length covers full extent of the Colville basin. Similarly, the southern part of sections represents the Brooks Range thrust belt which also shows good fit between observed and predicted anomalies. The rapid minute fluctuations in the red curve might notable in the wedge area are possibly due to anomalies calculated with high resolution deflection model.

The results of geophysical analysis are also examined and shown in (Figure 18 and 19). In addition to observed (black) and flexure model calculated (red) anomalies, the free-air anomalies calculated with seismic Moho depth (orange) are shown on three south-to-north cross-sections (Figure 19) in the study area.

Particularly the wedge area has good overall correlation of both calculations with the observed anomalies. However, there is some notable mismatch of about less than 40 mGal between the observed and calculated anomalies from seismic Moho data specifically in the basin area. This mismatch is very likely due to errors introduced by the interpolation technique used to build 3D model from the initial datasets, and the lateral variations of crustal and mantle densities which are ignored in the calculation of Moho from seismic datasets.

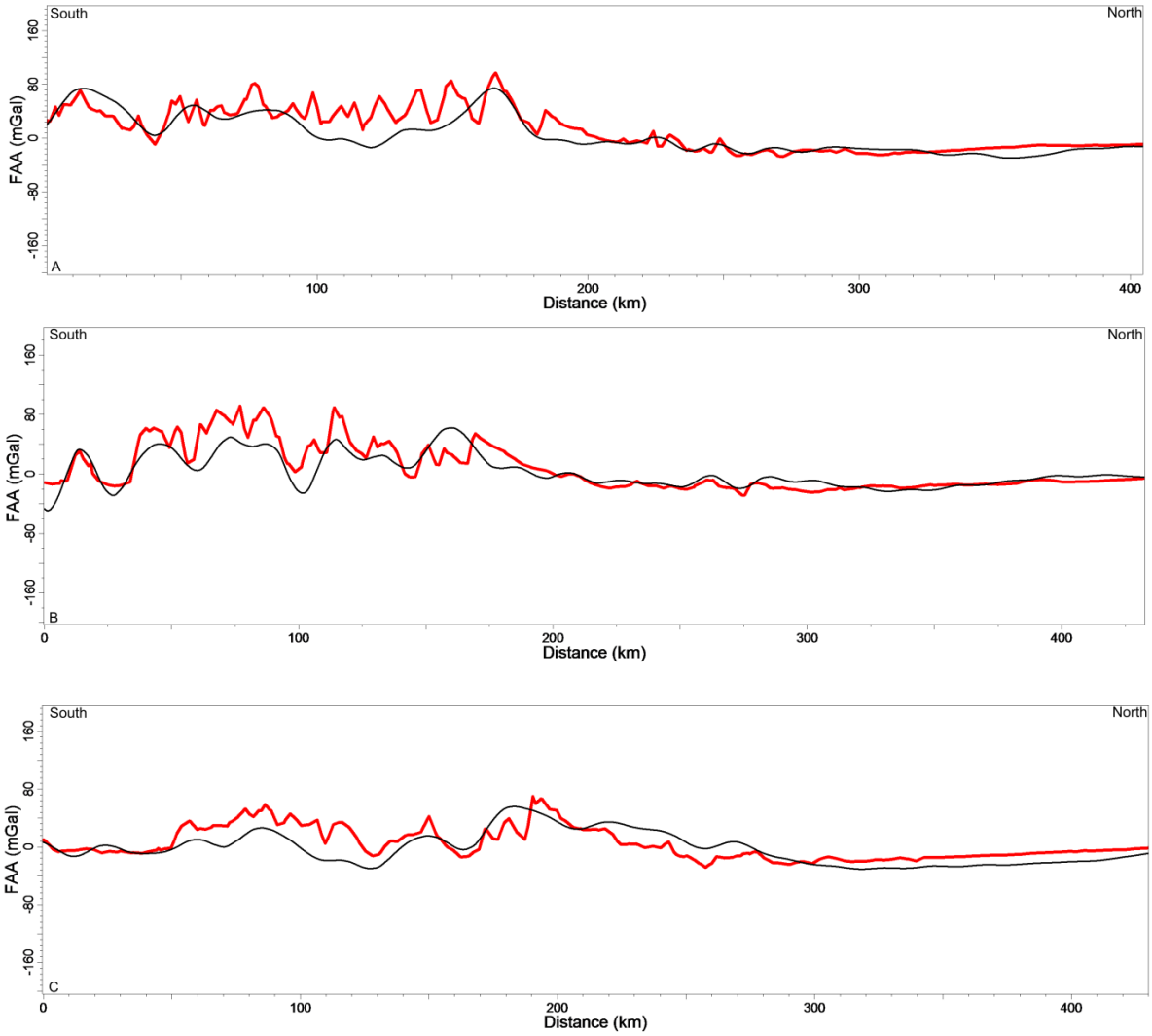

Figure 17. A comparison between observed FAA (black Curve; Bonvalot et al., 2012) and predicted FAA (red curve) along the sections A, B, and C. Location of sections are shown in Figure 13 inset map.

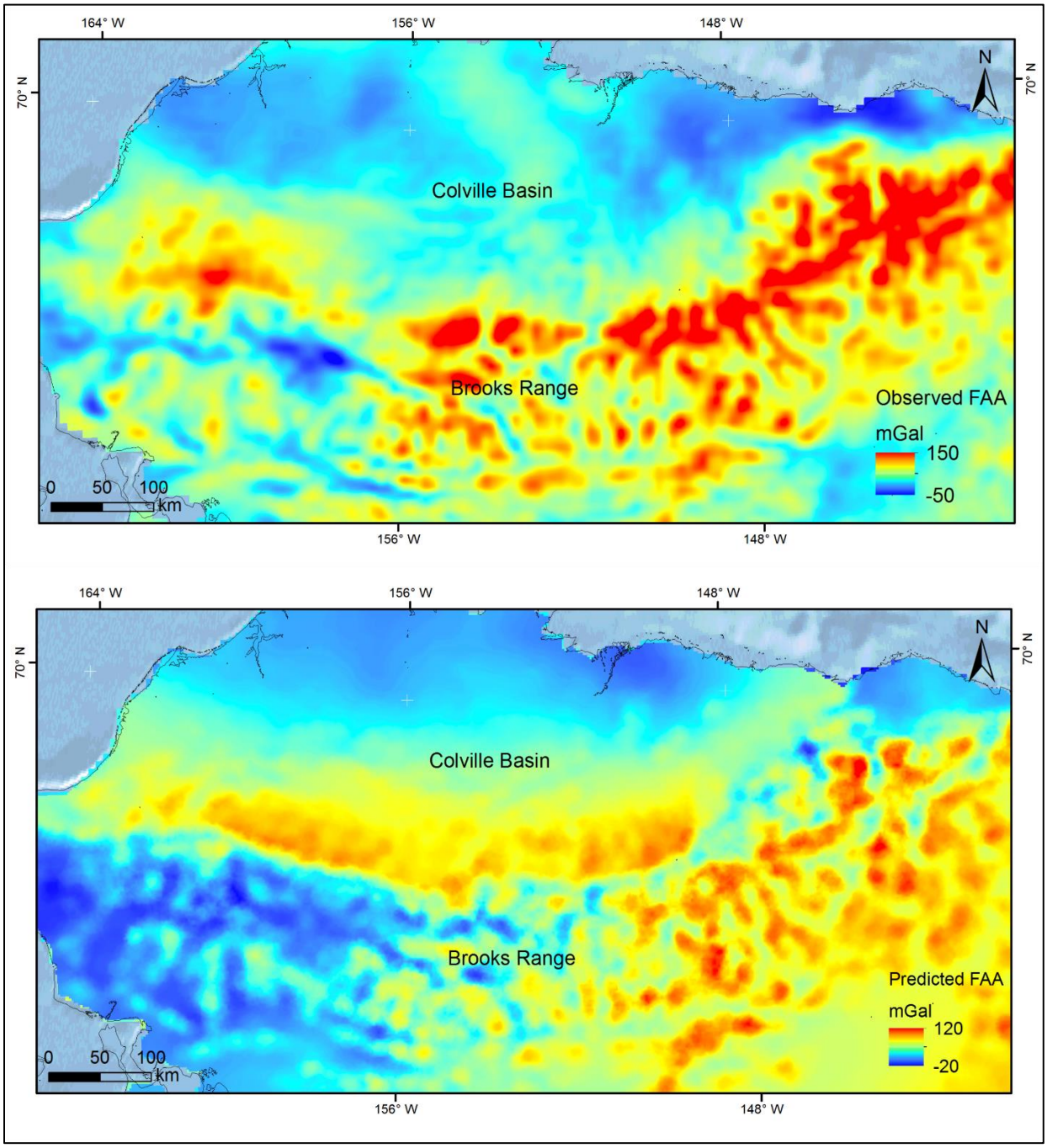

Figure 18. Upper part (Observed) and lower part (predicted from Moho boundary) published by (Torne et al., 2020) free-air anomalies (FAA). Brooks Range is characterized by particularly closer to zero anomalies (yellow) in the main thrust belt except for high values (red) where the belt extends further into the present-day shelf. Colville basin has typical foreland basin low anomaly

response (blue color). Overall slight misfit occurs between observed and predicted FAA when Moho boundary is used.

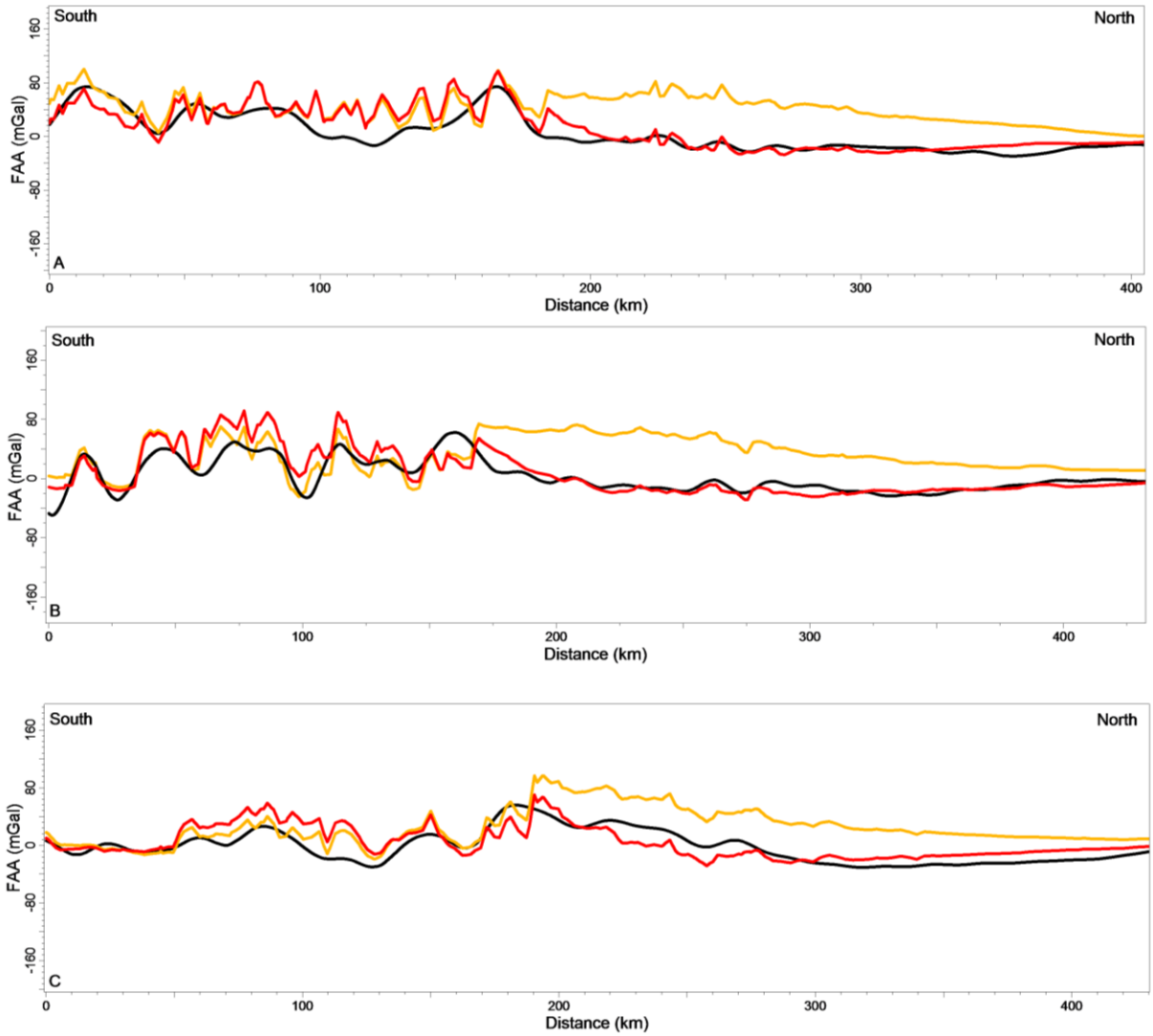

Figure 19. A comparison between observed FAA (black Curve; Bonvalot et al., 2012) with calculated FAA from seismic Moho (orange) (Torne et al., 2020) and deflection model (red) (this study) along the sections A, B and C. Location of sections are shown in Figure 13 inset map.

To ensure better correlation between observed basin flexure and the FAA, a model of the Moho geometry is determined considering it was initially flat and deformed as predicted by the flexural model. Considering undeformed crustal thickness of 37 km, the calculated Moho boundary from the flexural model is shown in (Figure 20 and 21). It shows a south to north cross-section spanning

about 250 km of Colville basin. The black curve represents the seismic derived Moho boundary and green represents Moho estimated with flexural model. A notable convergence of two curves in southern part of the section is probably due to over-estimation of flexure model. The southern part of the Colville basin experienced post-collisional deformation and as such the model showed a decrease in depth of foreland close to Brooks Range. Since the green curve (i.e. Moho estimated from flexure model) follows the same trend as the foreland geometry, it also decreases in depth whereas the observed Moho continues increasing in depth. Seismic derived Moho (Torne et al., 2020) is constrained by sparse P and S wave receiver functions and thus shows perturbations in the geometry which could be due to several reasons related to acquired seismic data and the interpolation techniques used. In an elastic bending plate, the curvature angle is expected to be same for upper and lower edges of the plate, therefore the estimated Moho boundary represents the correct subsurface geometry of Moho at least in northern part of the Colville basin.

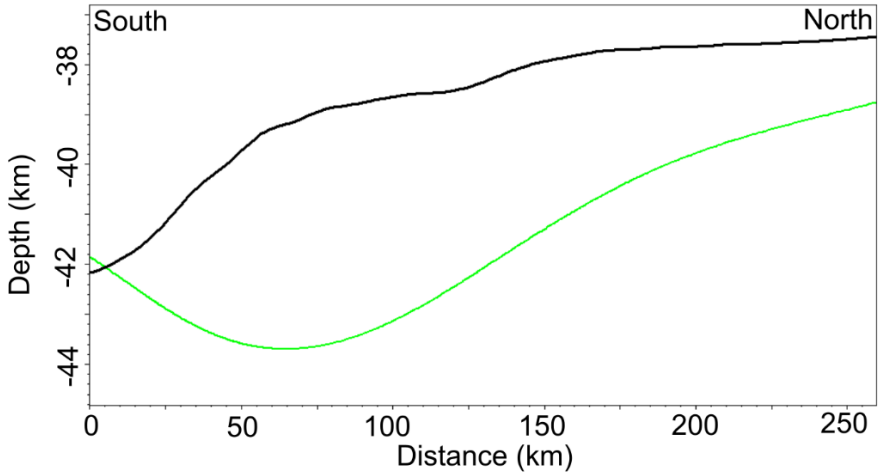

Figure 20. A comparison between observed Moho depth derived from seismic broadband (black) (Torne et al., 2020) and the Moho depths derived from the flexural model (green). Location of the section is shown in Figure 13.

The geophysical analysis supports and validates the results of flexural model of Colville foreland basin. The free-air gravity anomalies calculated by the flexural deflection model are very well correlated with observed gravity anomalies with maximum misfit of only 27 mGal. Since the gravity anomalies derived from the deflection model fits well to the observed gravity anomalies, it can be concluded that the estimated 16 km effective elastic thickness of the lithosphere is indeed an accurate representation of elastic strength of the lithosphere.

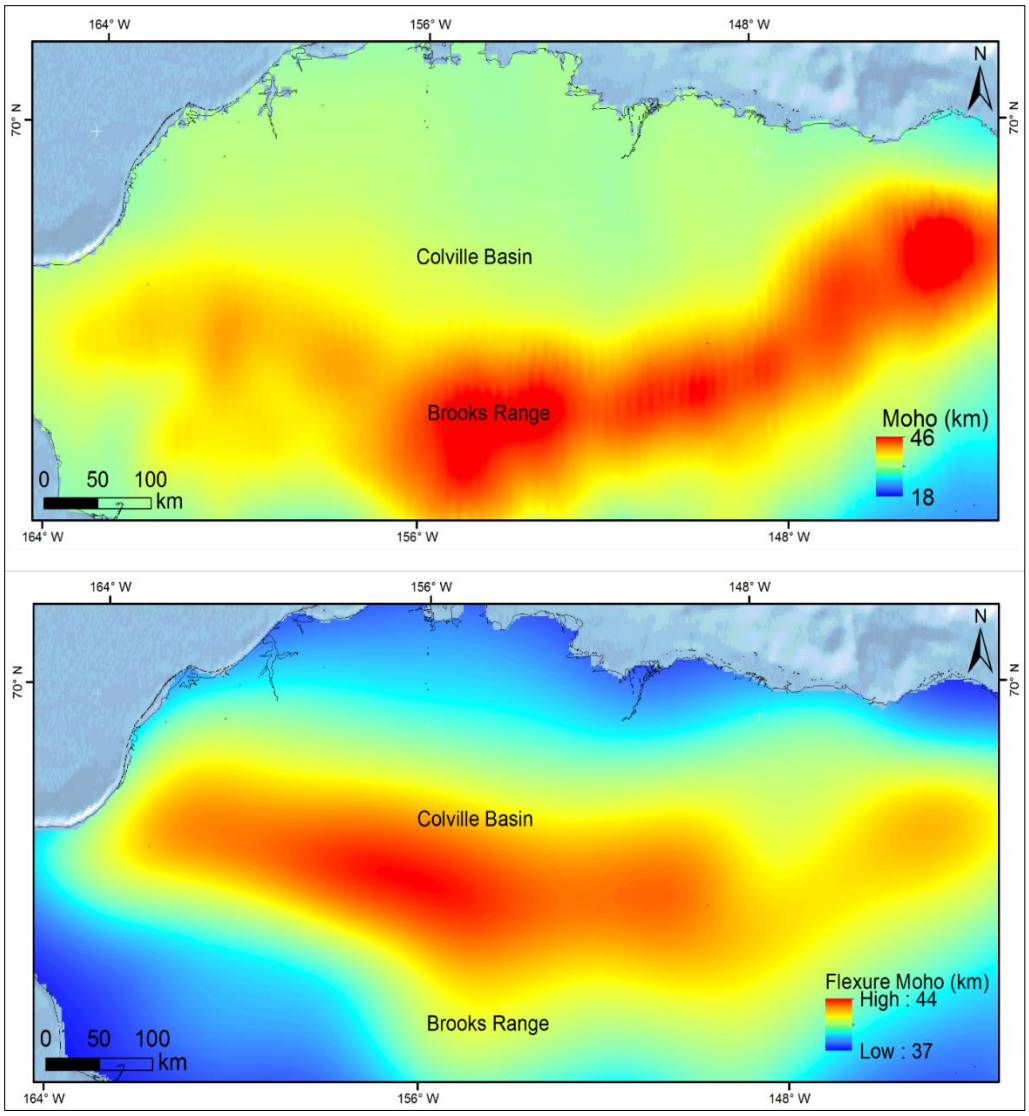

Figure 21. Upper panel (observed) and lower panel (predicted from flexural model) show Moho depth map.

5.5 Earthquake Observation

Geodynamic, lithospheric and tectonic studies can benefit a lot from the available opensource earthquake catalogs. Similar to earthquake seismic monitors of Incorporated Research Institutions for Seismology (IRIS), ZMAP (Wiemer, 2001) is also a seismological catalog of earthquakes with a very easy-to-use graphical user interface (GUI). This catalog serves as a tool to extract hundreds of thousands of earthquakes from any part of the world. The gathered data is efficiently categorized in map view and histograms that can be used for various forms of analyses. Using the mapping toolbox of MATLAB, ZMAP (Wiemer, 2001) has been utilized to analyze trends of seismicity in northern Alaska region.

The earthquakes occur in the uppermost part of brittle and competent layer of crustal lithosphere whose thickness is termed as seismogenic thickness or Ts. The seismogenic layer is usually about < 20 km with exceptions to the subduction zones where deep earthquakes (~40 km) can also occur. The strength of the continental lithosphere is likely to be contained within the seismogenic layer (Maggi et al., 2000), Earthquakes may extend deeper, into the brittle part of the sub-crustal mantle on major faults, in regions of high curvature or high bending stresses (Watts and Burov, 2003). On the other hand, the effective elastic thickness supports both the ductile and brittle strength of the lithosphere.

The objective of this analysis is to find distribution of most frequent earthquakes as function of their depth of origins. To this purpose only high magnitude earthquakes are considered since we need to find out at what depth the crust of northern Alaska behaves as aseismic. The representation

of huge amount of data is achieved by binning the earthquake events that are closer to each other into 5 km bins. The results are summarized in (Figure 22) which shows a histogram of frequency distribution of a total of 752 seismic events with large magnitude ($\geq 4\ to \leq 6.3$) versus depth of events. The events are obtained from 1960 to present. In northern Alaska, the analysis of earthquake observation shows that the maximum number of earthquake frequency dissipates at depths between 10 and 15 km (see Figure 23). This observation further validates the accuracy of the flexural model of Colville basin through which the elastic thickness is also estimated to be 16 km. Frequency of earthquakes increase at a larger depth (ca. 30 to 35 km) that roughly matches with the Moho depth in the area.

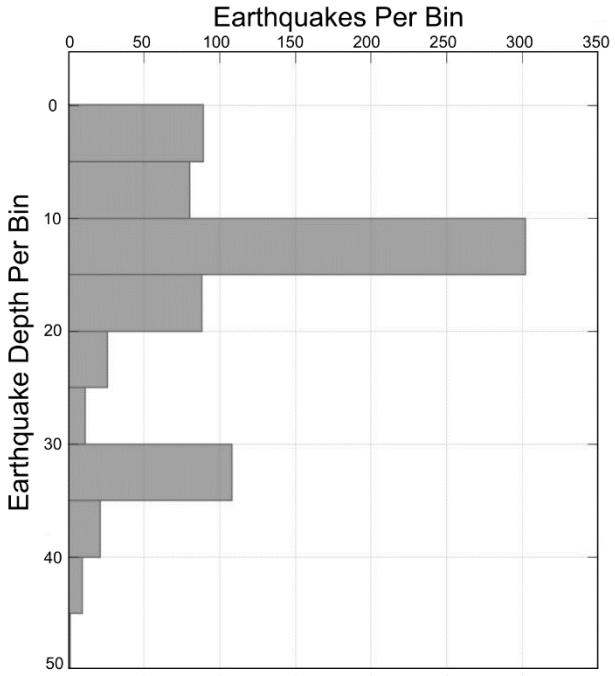

Figure 22. Frequency distribution chart showing the maximum depth of most frequent earthquakes near the Brooks Range and Colville basin dissipates at 20 km depth.

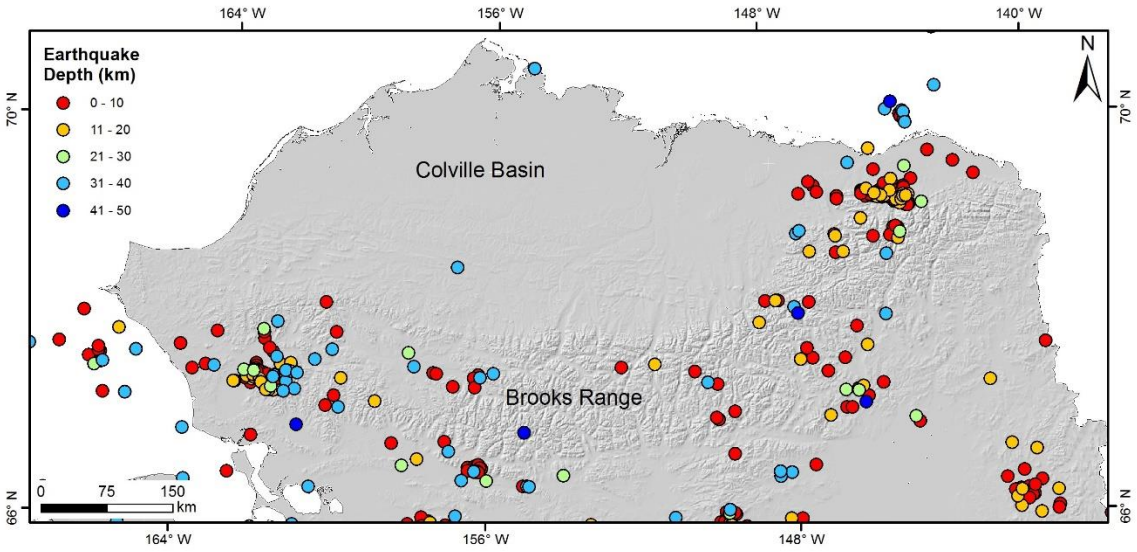

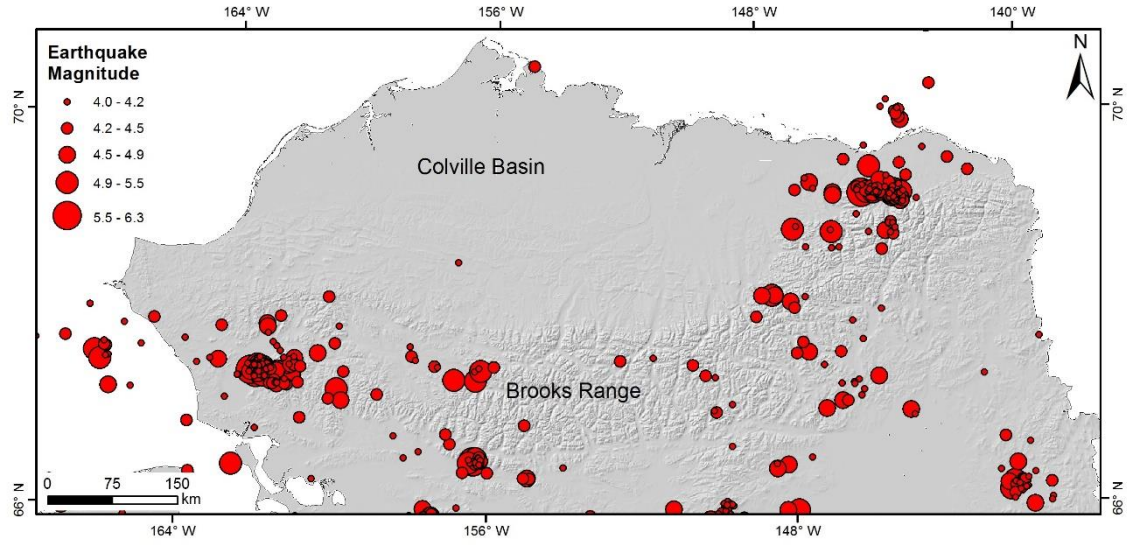

Figure 23. Upper panel shows locations of earthquakes with their corresponding depth. Lower panel shows corresponding magnitude of earthquakes.

CHAPTER 6

CONCLUSION

The elastic thickness of the lithosphere is an essential feature of plate geomechanics. In this study a simple 3D flexural model is adopted to quantitatively evaluate the elastic properties of the lithosphere in the northern Alaska region. The model is used to calculates the geometry of the Colville basin that is correlated to the observed basin geometry. The results indicate that a simple flexural model can very well reconstruct the post-collisional down warping of the Arctic Alaska plate in response to the Brooks Range orogeny.

3D flexure model is a first attempt to model flexure of the Colville foreland basin as previous flexural studies used only 2D methods. Using the gravity and topographic data, previous study indicated the presence of a subsurface dynamic load possibly induced by the subducting plate and estimated the elastic thickness to be 65 km. In contrast, this study produces a flexural model of the Colville basin that best fit to present-day geometry of the Colville basin with a misfit error of only 225 m or in another word error of calculation is less than 3%. The resulting value of the elastic thickness (16 km) is low by a very large magnitude. Since the load from the Brooks Range and the sediments of the Colville basin models an accurate deflection of the Colville basin that is well correlated with the present-day basin geometry, there is no need to invoke an additional subsurface dynamic load as inferred previously. It is important to note that the modeling approach is sensitive to several physical and geological parameters, that causes the mismatch between observed and predicted foreland depths. The observed misfit of this model is mainly influenced by post-

collisional contractional deformation and thrust front propagation, which significantly deformed the southern part of the foreland.

Results of this study are further supported by the analysis of the earthquake's depths in the northern Alaska region. In this region, most frequent earthquakes dissipate near 20 km depth. In other words, at 20 km depth the crust behaves aseismic and does not transmit significant stresses below this depth. From this observation, it can be inferred that the elastic thickness of the lithosphere is less likely to be greater than this depth. In addition, the computed elastic thickness from the flexural model i.e. 16 km also agrees to the observation of the earthquakes.

The geophysical investigations have provided an additional validity to the flexural model obtained in this study. The geophysical analysis includes calculations of the free-air surface gravity anomalies from the flexural modeling results and as well as the observed Moho boundary data compiled with broadband seismic. Comparison of gravity anomalies with the observed gravity anomalies shows an excellent correlation of anomalies for the wedge and the basin area. The maximum error between the observed and predicted free-air anomalies from the flexural model is only 27 mGal. This can be translated into validation of elastic parameters i.e. the elastic thickness derived from the flexural model. In other word, the flexure model produces the similar gravity anomalies as observed from direct gravity measurements. Analysis of gravity anomalies derived from the Moho boundary data also agrees with the observed anomalies, however, the misfit error is large (73 mGal) as compared to gravity anomalies from flexural model.

High values of the elastic thickness are generally associated with cold and strong lithosphere. With calculated 16 km elastic thickness it can be concluded that the lithosphere under the northern Alaska is relatively weak and hot. The elastic thickness of the lithosphere also depends upon the thermal gradient and composition of the lithosphere. To further understand the dynamics of the lithosphere in northern Alaska, spatial variations of the elastic thickness can be analyzed in future work. This would aid in better understanding of the tectonic and structural development of the region.

REFERENCES

Beaumont, C., 1981, Foreland basins: Geophysical Journal International, v. 65, no. 2, p. 291–329, doi:10.1111/j.1365-246X.1981.tb02715.x.

Beniest, A., 2018, From continental rifting to conjugate margins: insights from analogue and numerical modelling.

Bird, K. J., 2001, Framework geology, petroleum system, and play concepts of the National Petroleum Reserve - Alaska: doi:10.2110/cor.01.21.

Bird, K. J., and D. W. Houseknecht, 2011, Chapter 32 Geology and petroleum potential of the Arctic Alaska petroleum province: Geological Society, London, Memoirs, v. 35, no. 1, p. 485–499, doi:10.1144/M35.32.

Bonvalot, S., G. Balmino, A. Briais, M. Kuhn, A. Peyrefitte, N. Vales, R. Biancale, G. Gabalda, and F. Reinquin, 2012, World Gravity Map: a set of global complete spherical Bouguer and isostatic anomaly maps and grids: v. 14, p. 11091.

Brown, C. D., and R. J. Phillips, 2000, Crust-mantle decoupling by flexure of continental lithosphere: Journal of Geophysical Research: Solid Earth, v. 105, no. B6, p. 13221–13237, doi:10.1029/2000JB900069.

Burov, E., and M. Diament, 1996, Isostasy, equivalent elastic thickness, and inelastic rheology of continents and oceans: Geology, v. 24, no. 5, p. 419–422, doi:10.1130/0091-7613(1996)024<0419:IEETAI>2.3.CO;2.

Burov, E. B., and M. Diament, 1995, The effective elastic thickness (T e) of continental lithosphere: What does it really mean? Journal of Geophysical Research: Solid Earth, v. 100, no. B3, p. 3905–3927, doi:10.1029/94JB02770.

DeCelles, P. G., 2012, Foreland Basin Systems Revisited: Variations in Response to Tectonic Settings, *in* Tectonics of Sedimentary Basins: John Wiley & Sons, Ltd, p. 405–426, doi:10.1002/9781444347166.ch20.

DeCelles, P. G., and K. A. Giles, 1996, Foreland basin systems: Basin Research, v. 8, no. 2, p. 105–123, doi:10.1046/j.1365-2117.1996.01491.x.

Grantz, A., and S. D. May, 1982, Rifting his-tory and structural development of the continental margin north of Alaska: p. 77–100.

Grantz, A., S. D. May, and P. E. Hart, 1994, Geology of the Arctic continental margin of Alaska, *in* G. Plafker, and H. C. Berg, eds., The Geology of Alaska: Boulder, Colorado, Geological Society of America, p. 17–48, doi:10.1130/DNAG-GNA-G1.17.

Kearey, P., K. A. Klepeis, and F. J. Vine, 2009, Global tectonics: Oxford ; Chichester, West Sussex ; Hoboken, NJ, Wiley-Blackwell, 482 p.

Lowry, A. R., and R. B. Smith, 1995, Strength and rheology of the western U.S. Cordillera: Journal of Geophysical Research: Solid Earth, v. 100, no. B9, p. 17947–17963, doi:10.1029/95JB00747.

Maggi, A., J. A. Jackson, D. McKenzie, and K. Priestley, 2000, Earthquake focal depths, effective elastic thickness, and the strength of the continental lithosphere: Geology, v. 28, no. 6, p. 495–498, doi:10.1130/0091-7613(2000)28<495:EFDEET>2.0.CO;2.

McKenzie, D., and D. Fairhead, 1997, Estimates of the effective elastic thickness of the continental lithosphere from Bouguer and free air gravity anomalies: Journal of Geophysical Research: Solid Earth, v. 102, no. B12, p. 27523–27552, doi:10.1029/97JB02481.

Miller, T. P., 1994, Pre-Cenozoic plutonic rocks in mainland Alaska, *in* G. Plafker, and H. C. Berg, eds., The Geology of Alaska: Boulder, Colorado, Geological Society of America, p. 535–554, doi:10.1130/DNAG-GNA-G1.535.

Moore, T. E., and S. E. Box, 2016, Age, distribution and style of deformation in Alaska north of 60°N: Implications for assembly of Alaska: Tectonophysics, v. 691, p. 133–170, doi:10.1016/j.tecto.2016.06.025.

Moore, T. E., W. K. Wallace, K. J. Bird, S. M. Karl, C. G. Mull, and J. T. Dillon, 1994, Geology of northern Alaska, *in* G. Plafker, and H. C. Berg, eds., The Geology of Alaska: Boulder, Colorado, Geological Society of America, p. 49–140, doi:10.1130/DNAG-GNA-G1.49.

Mull, C. G., 1982, Tectonic Evolution and Structural Style of the Brooks Range, Alaska: An Illustrated Summary.

Nunn, J. A., M. Czerniak, and R. H. Pilger, 1987, Constraints on the structure of Brooks Range and Colville Basin, northern Alaska, from flexure and gravity analysis: Tectonics, v. 6, no. 5, p. 603–617, doi:10.1029/TC006i005p00603.

Patton, W. W., and S. E. Box, 1989, Tectonic setting of the Yukon-Koyukuk Basin and its borderlands, western Alaska: Journal of Geophysical Research: Solid Earth, v. 94, no. B11, p. 15807–15820, doi:10.1029/JB094iB11p15807.

Patton, W. W., Stephen. E. Box, and D. J. Grybeck, 1994, Ophiolites and other mafic-ultramafic complexes in Alaska, *in* G. Plafker, and H. C. Berg, eds., The Geology of Alaska: Boulder, Colorado, Geological Society of America, p. 671–686, doi:10.1130/DNAG-GNA-G1.671.

Pérez-Gussinyé, M., M. Metois, M. Fernández, J. Vergés, J. Fullea, and A. R. Lowry, 2009, Effective elastic thickness of Africa and its relationship to other proxies for lithospheric structure and surface tectonics: Earth and Planetary Science Letters, v. 287, no. 1, p. 152–167, doi:10.1016/j.epsl.2009.08.004.

Pirouz, M., J.-P. Avouac, A. Gualandi, J. Hassanzadeh, and P. Sternai, 2017, Flexural bending of the Zagros foreland basin: Geophysical Journal International, v. 210, no. 3, p. 1659–1680, doi:10.1093/gji/ggx252.

Plafker, G., and H. C. Berg, 1994, Overview of the geology and tectonic evolution of Alaska, *in* The Geology of Alaska: Boulder, Colorado, Geological Society of America, p. 989–1021, doi:10.1130/DNAG-GNA-G1.989.

Stier, N. E., C. D. Connors, and D. W. Houseknecht, 2014, Influence of the Kingak Shale ultimate shelf margin on frontal structures of the Brooks Range in the National Petroleum Reserve in Alaska, USGS Numbered Series 2014–5056: Reston, VA, U.S. Geological Survey, Scientific Investigations Report, 20 p.

Torne, M., I. Jiménez–Munt, J. Vergés, M. Fernàndez, A. Carballo, and M. Jadamec, 2020, Regional crustal and lithospheric thickness model for Alaska, the Chukchi shelf, and the inner and outer bering shelves: Geophysical Journal International, v. 220, no. 1, p. 522–540, doi:10.1093/gji/ggz424.

Turcotte, D. L., and G. Schubert, 2002, Geodynamics - 2nd Edition: 472 p., doi:10.2277/0521661862.

U.S. Geological Survey, 2005, Elevation derivatives for national applications: U.S. Geological Survey, Fact Sheet.

Watts, A. B., 1978, An analysis of isostasy in the world's oceans 1. Hawaiian-Emperor Seamount Chain: Journal of Geophysical Research: Solid Earth, v. 83, no. B12, p. 5989–6004, doi:10.1029/JB083iB12p05989.

Watts, A. B., 2001, Isostasy and flexure of the lithosphere: Cambridge ; New York, Cambridge University Press, 458 p.

Watts, A. B., and E. B. Burov, 2003, Lithospheric strength and its relationship to the elastic and seismogenic layer thickness: Earth and Planetary Science Letters, v. 213, no. 1, p. 113–131, doi:10.1016/S0012-821X(03)00289-9.

Wiemer, S., 2001, A Software Package to Analyze Seismicity: ZMAP: Seismological Research Letters, v. 72, no. 3, p. 373–382, doi:10.1785/gssrl.72.3.373.

BIOGRAPHICAL SKETCH

Muhammad Hassan Quddusi was born in Karachi, Pakistan. After completing high school in 2010, Hassan entered Bahria University in Karachi, Pakistan. He received a Bachelor of Science degree in Geophysics from Bahria University in August 2014. He then completed a Master of Science Degree in Geophysics from Bahria University and started his career in the oil and gas industry as a Geophysicist-Intern. After moving to the United States, Hassan wanted to pursue his career in the oil and gas industry and wanted to pursue advanced research in the field of geosciences. In August 2017, he entered the Geoscience graduate program at The University of Texas at Dallas. He is married to Arooba Hassan and is a proud father of his first child, Musa, who was born while he attended his graduate school.

CURRICULUM VITAE

Education

Master of Science (MS) in Geosciences
The University of Texas at Dallas
Fall 2017 – Spring 2020

Master of Science (MS) in Geophysics
Bahria University, Karachi, Pakistan
Fall 2014 – Fall 2016

Bachelor of Science (BS) in Geophysics
Bahria University, Karachi, Pakistan
Fall 2010 – Spring 2014

Experience

Graduate Teaching Assistant, UT Dallas, Dept. of Geosciences

Fall 2019 – Spring 2020

Professional Affiliations

- Coordinator AAPG Student Chapter UTD 2018
- American Association of Petroleum Geologists

Honors and Awards

- Dallas Geological Society Scholarship
- NSM Geo Gaynor Opportunity Award

Abstracts

Quddusi, Muhammad Hassan and Pirouz, Mortaza, 2020, 3-D Geometrical Reconstruction and Flexural Modeling of Colville Foreland Basin, Northern Alaska: Geological Society of America Abstracts with Programs. Vol. 52, No. 1 doi: 10.1130/abs/2020SC-343738